Molecular Pharmacology Fast Forward. Published on January 25, 2006 as doi:10.1124/mol.105.018580

Title page

Title:

Subunit dependencies of NMDA receptor-induced AMPA receptor internalization*

Authors:

C. M. Tigaret, A. Thalhammer, G. F. Rast, C. G. Specht, Y. P. Auberson, M. G. Stewart, and R. Schoepfer

Primary laboratory of origin:

Laboratory for Molecular Pharmacology, Department of Pharmacology, UCL, Gower Street, London WC1E 6BT, UK

Affiliation:

C.M.T, A.T., G.F.R., C.G.S, R.S.: Laboratory for Molecular Pharmacology, Department of Pharmacology, University College London, Gower Street, London WC1E 6BT, UK.

Y.P.A: Novartis Institutes for Biomedical Research, Novartis Pharma AG, CH-4002 Basel, Switzerland.

M.G.S.: Department of Biological Sciences, The Open University, Milton Keynes, MK7 6AA, UK.

Present Address for C.G.S.: Stanford University, Department of Psychiatry & Behavioral Sciences, Stanford, CA 94304, USA

Molecular Pharmacology Fast Forward. Published on January 25, 2006 as DOI: 10.1124/mol.105.018580
This article has not been copyedited and formatted. The final version may differ from this version.

Running title page

Running title: NR2B-dependent internalization of GluR2.

Corresponding author:

Ralf Schoepfer, Laboratory for Molecular Pharmacology, Department of Pharmacology, UCL, Gower Street, London WC1E 6BT, UK; Tel +44-20-76797242, Fax +44-20-76797245, E-mail: r.schoepfer@ucl.ac.uk

Number of text pages: 36.

Number of tables*:* 0.

Number of figures: 6.

Number of references: 40.

Number of words in the Abstract: 194.

Number of words in the Introduction: 451.

Number of words in the Discussion: 1163.

Abbreviations:

AMPA, alpha-amino-3-hydroxy-5-methyl-4-isoxazolepropionic acid; APV, 2-amino-5-phosphonopentanoic acid; AMPAR, AMPA receptor; (E)GFP, (enhanced) green fluorescent protein; E-GluR2-S: EGFP-tagged GluR2, short C-terminus; E-GluR2-L: EGFP-tagged GluR2, long C-terminus; HEPES, 4-(2-hydroxyethyl)piperazine-1-ethanesulfonic acid; HS, horse serum; IFP, ifenprodil; KA, kainate; NMDA, N-methyl-D-aspartate; NMDAR, NMDA receptor; NVP, NVP-AAM077; Ro, Ro25-6981; TTX, tetrodotoxin.

Molecular Pharmacology Fast Forward. Published on January 25, 2006 as DOI: 10.1124/mol.105.018580
This article has not been copyedited and formatted. The final version may differ from this version.

Abstract

NMDA receptor (NMDAR) activity regulates the net number of AMPA receptors (AMPAR) at the cell surface by modulating the balance between AMPAR membrane insertion and endocytosis. Here we addressed the role of NMDAR subtypes and of NMDAR-mediated Ca^{2+} influx in the NMDAR-induced endocytosis of GluR2-containing AMPARs in primary murine hippocampal neurons. We found that NMDAR activation enhanced the endocytosis of AMPARs containing the GluR2 splice variants with short, but not long, cytoplasmic tails. NMDA-induced GluR2 endocytosis was completely inhibited by pharmacological block of NR2B-containing NMDARs. In turn, preferential block of NR2A-containing NMDARs did not affect NMDA-induced AMPAR endocytosis indicating that AMPAR internalization is controlled by a restricted set of NMDARs. The NMDA-induced GluR2 internalization was also observed in the absence of extracellular Na^{+} ions, suggesting that membrane depolarization is not a prerequisite for this effect. Furthermore, the activation of Ca^{2+}-impermeable NMDARs containing the mutant NR1(N598R) subunit failed to enhance AMPARs endocytosis, indicating a requirement of Ca^{2+} influx directly through the NMDAR channels. In summary, our findings suggest that the NMDAR-induced selective internalization of short C-terminal GluR2-containing AMPARs requires a Ca^{2+} signal that originates from NMDAR channels and is processed in an NMDAR subtype-restricted manner.

Molecular Pharmacology Fast Forward. Published on January 25, 2006 as DOI: 10.1124/mol.105.018580
This article has not been copyedited and formatted. The final version may differ from this version.

Introduction

The regulation of AMPAR membrane density by NMDAR activity is a key mechanism for the expression of NMDAR-dependent plasticity via the membrane insertion or endocytosis of AMPARs (Kim et al., 2005; Malenka and Bear, 2004; Zhu et al., 2005). The early determinants in the NMDAR signaling leading to AMPAR internalization are largely unknown.

AMPAR channels are formed by hetero-tetrameric combinations of GluR1-4 subunits that determine the electrophysiological properties of AMPARs and govern their trafficking via C-terminal cytoplasmic domains (Collingridge et al., 2004; Sheng and Kim, 2002). The GluR2 subunit is particularly relevant in that it renders AMPAR channels impermeable to Ca^{2+} (Dingledine et al., 1999) and is present in the predominant AMPAR heteromers of pyramidal hippocampal neurons (Wenthold et al., 1996). The cytoplasmic tail of the short GluR2 C-terminal splice variant "drives" the constitutive recycling and the NMDAR-induced internalization of AMPARs (Lee et al., 2004; Shi et al., 2001). In contrast, the long GluR2 C-terminal splice variant contributes to AMPAR membrane insertion (Kolleker et al., 2003), as do GluR1 and the long C-terminal splice variant of GluR4 (Hayashi et al., 2000; Zhu et al., 2000), or to AMPAR removal during depotentiation (Zhu et al., 2005). The contribution of the long GluR2 C-terminal splice variant to AMPAR endocytosis induced by acute NMDAR activation remains, however, unknown.

NMDAR subtypes are hetero-tetrameric complexes typically formed by NR1 and NR2A-D subunits (Wenthold et al., 2003). In the hippocampus and the neocortex NR2B predominates in early postnatal life, whereas NR2A is gradually expressed during the first two postnatal weeks, resulting in diheteromeric (NR1/NR2A, NR1/NR2B) and triheteromeric (NR1/NR2A/NR2B) receptor subtypes (Kew et al., 1998). This developmental profile is parallelled *in vitro* (Li et al., 2002).

Molecular Pharmacology Fast Forward. Published on January 25, 2006 as DOI: 10.1124/mol.105.018580
This article has not been copyedited and formatted. The final version may differ from this version.

Both NMDAR-dependent synaptic long-term potentiation (LTP) and depression (LTD), and the NMDAR-induced membrane insertion or removal of AMPARs require a postsynaptic Ca^{2+} transient elicited by NMDAR activation (Lisman, 1989; Sheng and Kim, 2002). Beyond the model in which the Ca^{2+} signal kinetics directs the balance of this duality (Lisman, 1989), recent observations suggest that the NR2 subunit composition of NMDAR complexes plays a decisive role in the effects downstream of NMDAR activation (Kim et al., 2005; Liu et al., 2004; Massey et al., 2004).

Here, we investigated the role of NMDAR subtypes in the NMDA-induced endocytosis of surface AMPARs containing N-terminally EGFP-tagged GluR2 expressed in hippocampal cultures using a Sindbis virus-derived system. NMDAR activation enhanced the intracellular accumulation of AMPARs containing the short, but not the long C-terminal splice variant of GluR2. This effect was initiated by NR2B- but not NR2A-containing NMDARs and required Ca^{2+} influx through the activated NMDAR channels. We propose that NR2B-specific processing of the Ca^{2+} signals carried by NMDARs constitute an early step in the regulated AMPAR endocytosis.

Molecular Pharmacology Fast Forward. Published on January 25, 2006 as DOI: 10.1124/mol.105.018580
This article has not been copyedited and formatted. The final version may differ from this version.

Materials and Methods

Materials

All chemicals and drugs were obtained from Sigma (Poole, Dorset, UK), unless specified otherwise.

Animal procedures

Procedures were performed according to the Animals Scientific Procedures Act of 1986, under license of the Home Office. Animals were kept at the Biological Services Unit of the University College London.

Sindbis virus expression of recombinant E-GluR2 in cultured neurons.

We constructed an N-terminally EGFP-tagged GluR2 subunit following a strategy similar to that described by Shi et al. (1999). A multistep cloning procedure resulted in a construct containing from the 5' to the 3' end: the 5' UTR from *Xenopus* hemoglobin, rat GluR1 signal peptide and four amino acid residues beyond the signal-peptide-cleavage site, EGFP coding sequence from vector pEGFP-N1 (Clontech), rat GluR2 flop coding sequence from codon 21 onwards, and the Sindbis-specific 3' UTR and poly(A) tail from the SINrep(nsP2S726) plasmid (Kim et al., 2004). The relevant DNA sequences were confirmed by sequencing and submitted to EMBL as pGFP-GluR2-Sin (accession number AJ870439). For the generation of short and long C-terminal GluR2 splice variants, the respective sequences were amplified by RT-PCR from total brain mouse E17 RNA, encoding the amino acid residues from Y837KSR (TACAAGTCAAGGG) onwards through a sequence common to both splice variants (CCTTGAATTGTAAG, 130 bp beyond the STOP codon in the 3' UTR of the long splice variant), and shuttled into pGFP-GluR2-Sin. The splice variant-specific sense primers were 5'-TACAAGTCAAGGGCCGAGGCGAAACGAATGAAGGTGGCAAAGAAT (for GluR2 short), and 5'-TACAAGTCAAGGGCCGAGGCGAAACGAATGAAGATGACCTTGAGC

(for GluR2 long). The common antisense primer was 5'-CCTTGAATTGTAAGGAAAGATTACTCGAGGGCCTACGT.

pGFP-GluR2-Sin constructs with short and long C-terminal splice variants were shuttled into SINrep(nsP2S726) with *Xba* I and *Not* I, and recombinant Sindbis replicons were generated as described (Kim et al., 2004; Specht et al., 2005). Virions were harvested 24-36 h after transfection of 1 x 10^7 BHK-21 cells, typically yielding in the range of 10^6 infectious units/ml.

Primary mouse hippocampal neuron cultures.

Primary hippocampal cultures were generated from individual animals either at embryonic day 16 (E16) for NR1 mutant mice or otherwise at postnatal day 0 (P0), as described (Specht et al., 2005), and fed weekly by replacing half of the culture medium with a freshly prepared one. Experiments were performed on cultures between days *in vitro* (DIV) 14-21. Cells expressing EGFP-tagged GluR2 were used 18-28 h after infection with Sindbis virions. Viral titers were adjusted to yield 20-30% green fluorescent cells.

Electrophysiology.

Cultures at DIV 14-21 were placed in a recording chamber and perfused at room temperature (RT, 20-25º C) with artificial CSF (aCSF) [in mM: 124 NaCl, 2.4 KCl, 2 $CaCl_2$, 2 $MgCl_2$, 1.2 NaH_2PO_4, 26 $NaHCO_3$, and 20 glucose, pH 7.4, saturated with 95% O2 + 5% CO_2], and containing 200 nM tetrodotoxin (TTX, Tocris, Northpoint, Avonmouth, UK), 10 µM bicuculline methiodide and 1 µM strychnine. Where necessary, infected cells were identified by their green fluorescence.

Rectification of kainate-induced AMPAR responses was determined in whole-cell voltage clamp mode by local superfusion of 100 µM kainate (KA) in aCSF, either by voltage ramps from -70 mV to 50 mV (0.1 mV/ms) at constant perfusion, or by holding at discrete potentials

Molecular Pharmacology Fast Forward. Published on January 25, 2006 as DOI: 10.1124/mol.105.018580
This article has not been copyedited and formatted. The final version may differ from this version.

and switching of superfusion. Series resistance was compensated at 80-95%. In the case of voltage ramps, leakage current was determined in the absence of agonist, and subtracted. Glass pipettes for whole-cell patch recordings (4-6 MΩ resistance) were filled with [in mM: 115 cesium methanesulfonate, 20 CsCl, 10 HEPES, 2.5 $MgCl_2$, 4 Na_2ATP, 0.4 Na_3GTP, 10 sodium phosphocreatine, 0.6 EGTA, 0.1 spermine, pH 7.25]. NMDA-induced responses were obtained in nominally Ca^{2+}- and Mg^{2+}-free aCSF, containing 20 µM DNQX, at –60 mV. aCSF containing 20 µM NMDA and 10 µM glycine was applied by bath perfusion. NMDAR antagonists ifenprodil (IFP, 10 µM), or NVP-AAM077 (NVP, 1 µM, Novartis Pharma, Basel, Switzerland) were pre-applied for 2 min and present during agonist application.

Data were collected using an Axopatch 200B amplifier, filtered at 5 kHz, digitized and streamed to disk, using CellWorks software (npi electronic, Tamm, Germany). Off-line analysis and graphs were produced using Igor Pro 4 (WaveMetrics, Lake Oswego OR), or Scilab 3.0 (Scilab Consortium, INRIA, France, http://scilabsoft.inria.fr).

Immunofluorescence protocol for GluR2 internalization.

To visualize the internalization of AMPARs containing either endogenous or recombinant EGFP-tagged GluR2 we used an antibody-feeding protocol (see Supplementary Table SI for a schematic protocol and duration of live antibody incubations). Antibodies were diluted in equilibrated culture medium containing 5% heat-inactivated horse serum (HS, GIBCO 26050-088). Live antibody incubations were followed by three washes (amounting to 1 min) in the same medium. The surface EGFP-tagged receptors were initially labeled live with unconjugated anti-GFP rabbit antiserum (ab290, Abcam, Cambridge, UK, 1:100) under normal culture conditions. For the activation of NMDARs, the cultures were washed (1 min) at RT in aCSF, then treated for 2 min with agonist as indicated in figure legends. Unstimulated controls consisted of cultures treated only with aCSF. After treatment, the cells were washed again in aCSF (1 min) and returned to normal culture conditions. Drugs were

Molecular Pharmacology Fast Forward. Published on January 25, 2006 as DOI: 10.1124/mol.105.018580
This article has not been copyedited and formatted. The final version may differ from this version.

applied in Mg^{2+}-free buffers, in the presence of 20 µM DNQX, 200 nM TTX, 10 µM bicuculline methiodide and 1 µM strychnine. When used, NMDAR antagonists (APV, IFP, Ro, or NVP) were pre-applied during the aCSF wash, and thus were present throughout the 3 min period (concentrations as indicated in figure legends). For the experiments in Fig. 4 A, HEPES-Ringer [in mM: NaCl, 126; KCl, 2.4; $CaCl_2$, 2; $MgCl_2$, 2; HEPES 5; pH 7.35] was used instead of aCSF, with sodium chloride substituted with choline chloride for solutions without sodium.

Cultures were then returned to normal conditions for the durations given in figure legends and Table SI, and surface and internalized EGFP-tagged GluR2 on the same cells were stained by successive application of secondary antibodies. To reveal the subpopulation of EGFP-tagged GluR2 still present at the cell surface, cultures were stained live with Cy5-conjugated goat anti-rabbit IgG (Jackson ImmunoResearch, West Grove, PA, USA, cat. no. 111-175-003, 15 µg/ml in HS-containing culture medium). After a brief wash in the same medium, the cultures were fixed (4% paraformaldehyde and 1% sucrose in PB: 0.1 M NaH_2PO_4, pH 7.5, 10 min), permeabilized and blocked with blocking solution (PB containing 0.3% Triton X-100 and 5% HS, 30 min). The internalized subpopulation of EGFP-tagged GluR2 was stained with a rhodamine (TRITC)-conjugated anti-rabbit IgG (Jackson ImmunoResearch, cat. no. 111-026-003, 15 µg/ml in blocking solution, 30 min). For the staining of presynaptic terminals, a mouse monoclonal anti-synaptophysin antibody (Chemicon, MAB5258-20UG, 10 µg/ml) was included in this step, and was followed by incubation with AMCA-conjugated goat anti-mouse IgG (Jackson ImmunoResearch, 115-155-146, 15 µg/ml). Cultures were finally washed in PB and mounted in Gel-Mount (Sigma, G-0918). When specified, nuclei were counterstained with Hoechst 33258 (Molecular Probes, Inc, 1 µg/ml in PBS) for 5 min at RT, prior to mounting.

Molecular Pharmacology Fast Forward. Published on January 25, 2006 as DOI: 10.1124/mol.105.018580
This article has not been copyedited and formatted. The final version may differ from this version.

The specificity of the anti-GFP immunostaining for the surface-targeted EGFP-tagged GluR2 was confirmed by the lack of GFP immunoreactivity in naïve cultures (i.e., not infected with EGFP-tagged GluR2 Sindbis virus), as shown in Supplementary Fig. S1. We also confirmed the ability of the Cy5-conjugated antibody to saturate the EGFP-tagged GluR2-anti-GFP immunocomplexes still present at the cell surface by performing a test immunostaining where Cy5- and TRITC-conjugated antibodies were successively applied live, before fixation. Under these circumstances, no signal was detected from the second, TRITC-conjugated antibody (Supplementary Fig. S2).

The internalization of the AMPARs containing native endogenous GluR2 subunit was visualized by a similar protocol, using a monoclonal antibody against the GluR2 N-terminal amino acids 175-430 (Chemicon, MAB397, 17 µg/ml ml in HS-containing culture medium) followed by Cy5-conjugated goat anti-mouse IgG (Jackson ImmunoResearch, West Grove, PA, USA, cat. no. 115-175-003, 15 µg/ml in HS-containing culture medium) and Cy3-conjugated goat anti-mouse IgG (Jackson ImmunoResearch, West Grove, PA, USA, cat. no. 115-165-003, 15 µg/ml in HS-containing culture medium) for surface and internalized GluR2, respectively. The specificity of anti-GluR2 antibody was confirmed by the lack of immunoreactivity on *Gria*$2^{-/-}$ neurons (data not shown).

Confocal microscopy and image analysis.

Multi-channel fluorescence confocal images were acquired on a LSM 510 Meta laser scanning confocal microscope (Carl Zeiss Ltd., UK) with an oil-immersion Plan-Apochromat objective (63x, NA 1.40). Excitation/emission filter wavelengths were (nm): 364/385 long-pass for AMCA and Hoechst 33258, 488/505-550 for EGFP, 543/568-610 for TRITC or Cy3 and 633/664-717 for Cy5. Fluorescence channels were acquired in sequential line-scan mode to minimize channel cross-talk. Pinholes were set to 1 Airy disk unit and acquisition parameters were adjusted close to full dynamic range, independently for each channel.

Molecular Pharmacology Fast Forward. Published on January 25, 2006 as DOI: 10.1124/mol.105.018580
This article has not been copyedited and formatted. The final version may differ from this version.

Confocal data were acquired blindly with respect to the experimental conditions, from neurons showing clear anti-GluR2 or green fluorescent cells with anti-EGFP immunofluorescent puncta in conventional fluorescence. The acquisition field (146 x 146 µm) was centered on the soma. Optical slices (20-50) were recorded with a resolution of 140 nm (lateral) and 240 nm (axial) and stored as multi-channel 16 bit image files.

Image analysis was performed separately on the three-dimensional fluorescence data sets for the Cy5 and TRITC channels using ImageJ software (Rasband, W. S., National Institutes of Health, Bethesda, MD, USA, http://rsb.info.nih.gov/ij/). Grayscale fluorescent images were converted to 32 bit floating point and were processed through a median filter to remove photomultiplier noise. In order to isolate immunofluorescent E-GluR2 puncta from the background, images were segmented using bi-level thresholding based on the gray level histogram. Threshold values were initially determined by the automatic threshold feature of ImageJ, based on an iterative algorithm and then were manually lowered under visual control to encompass all immunofluorescent puncta, which typically meant pixels above 1/10 of the maximum gray value in the image. Similar results were obtained with an automated thresholding algorithm based on gray level histogram entropy. Subsequently, one pixel-wide structures, were removed from the segmented images by one iteration of morphological opening. Images were analyzed blindly with respect to the experimental conditions.

The internalized fraction of GluR2 subunit was expressed quantitatively as the ratio between the count of thresholded voxels in the TRITC (for EGFP-tagged GluR2) or Cy3 (for the endogenous GluR2) channel and the sum of thresholded voxels in TRITC or Cy3 and Cy5 channels. The raw values for the internalized fraction in our experiments are given in the Supplementary Table SI. The data shown in the figures represent mean ± SEM of the internalization index obtained by normalizing the internalized fraction to the values obtained in unstimulated cells within each experimental group, as indicated in the legends. The

Molecular Pharmacology Fast Forward. Published on January 25, 2006 as DOI: 10.1124/mol.105.018580
This article has not been copyedited and formatted. The final version may differ from this version.

numbers of neurons used in the analysis are indicated in figure legends and in Supplemental Table SI and represent data from typically 3 coverslips for each condition. Illustrations show Z-projected fluorescence confocal stacks overlaid in pseudo-color using The GNU Image Manipulation Program (http://www.gimp.org/).

Molecular Pharmacology Fast Forward. Published on January 25, 2006 as DOI: 10.1124/mol.105.018580
This article has not been copyedited and formatted. The final version may differ from this version.

Results

N-terminally EGFP-tagged GluR2 reconstitutes the GluR2 phenotype in Gria2$^{-/-}$ neurons.

To visualize the subcellular distribution of GluR2-containing AMPARs, we constructed a recombinant N-terminally EGFP-tagged, short C-terminal splice variant GluR2 (E-GluR2-S), and expressed it in primary hippocampal neurons using a Sindbis virus-derived system. E-GluR2-S-expressing neurons exhibited finely grained somatodendritic fluorescence from the EGFP tag within 24 hours of infection. To confirm that our expression system delivered subunits that formed functional AMPAR channels, we analyzed the I-V relationship of whole-cell AMPAR currents in GluR2 knockout (*Gria2*$^{-/-}$) neurons infected with virus encoding E-GluR2-S.

Currents elicited with 100 μM kainate (KA) in uninfected wild-type neurons displayed a linear I-V relationship (Fig. 1 A). In contrast, whole-cell responses to KA in uninfected *Gria2*$^{-/-}$ neurons had the expected inward rectifying I-V relationship (Fig. 1 A) characteristic of the GluR2-lacking AMPARs in these animals (Jia et al., 1996). Expression of E-GluR2-S rescued the wild-type AMPAR phenotype in *Gria2*$^{-/-}$ neurons. KA responses from *Gria2*$^{-/-}$ neurons infected with E-GluR2-S virus had a near-linear I-V relationship (Fig. 1 A) with a rectification index of 0.4 ± 0.13 (Fig. 1 B), significantly different from uninfected *Gria2*$^{-/-}$ cells (0.06 ± 0.03, $p<0.05$) and near the values in uninfected wild-type neurons (0.72 ± 0.11).

These results demonstrate that our recombinant subunit was functional and was incorporated into newly synthesized AMPARs targeted at the cell surface. AMPAR subunits have been reported to form homomeric receptors when expressed *in vitro* (Shi et al., 2001). Homomeric GluR2 receptors typically yield agonist-induced currents one order of magnitude smaller than heteromeric GluR1/2 receptors (Keinanen et al., 1990). In our system however, currents elicited by KA in E-GluR2-S-expressing *Gria2*$^{-/-}$ neurons were comparable in amplitude to

Molecular Pharmacology Fast Forward. Published on January 25, 2006 as DOI: 10.1124/mol.105.018580
This article has not been copyedited and formatted. The final version may differ from this version.

those recorded from wild-type neurons where heteromeric AMPARs are natively predominant (-611.14 ± 166.4 pA and –756 ± 207.5 pA respectively, at –60 mV holding potential).

Taken together, this indicates the existence of heteromeric GluR1/E-GluR2-S receptors in infected *Gria2*$^{-/-}$ cells, possibly at a relative proportion similar to that of heteromeric GluR1/GluR2 in wild-type neurons.

NMDAR-induced E-GluR2-S AMPAR internalization.

We determined the internalization of E-GluR2-S AMPARs using a live antibody-feeding protocol (see Materials and Methods). Under confocal microscopy examination, the anti-GFP-stained cell surface E-GluR2-S appeared as abundant Cy5-fluorescent puncta decorating the soma and the dendritic arborizations, whereas the anti-GFP-stained E-GluR2-S that had been internalized after receptor activation as TRITC-fluorescent puncta located in the soma and dendritic shafts (Fig. 2A). Co-staining for the presynaptic marker synaptophysin revealed that most of the cell surface puncta were in the proximity of synaptic terminals (Fig. 5B).

Activation of NMDARs for 2 min with 20 μM NMDA and 10 μM Gly enhanced E-GluR2-S internalization above the constitutive levels of unstimulated cells, as early as 5 min after agonist washout (see Supplementary Fig. S3, and Supplementary Table SI rows 3-14). Twenty minutes after NMDAR activation, the E-GluR2-S endocytosis was enhanced by 2.31 ± 0.32 fold and was blocked by 50 μM APV (0.93 ± 0.08 times unstimulated controls, Fig. 2 B and Table SI row 70). A more intense stimulus (100 μM NMDA and 1μM Gly, for 2 min) enhanced the E-GluR2-S internalization with a similar time course and was blocked by 100 μM APV (Table SI rows 15-20, 71).

Molecular Pharmacology Fast Forward. Published on January 25, 2006 as DOI: 10.1124/mol.105.018580
This article has not been copyedited and formatted. The final version may differ from this version.

Strictly speaking this assay does not measure the amount of endocytosed receptors per se, but rather shows the amount of pre-labeled, formerly at the surface receptors which got internalized, but not recycled nor degraded before fixation. Kinetic studies, however, indicate that the measured signal is a valid representation of the actually internalized fraction, in particular at short incubation periods (Figs S3A, Fig 5A. and Lee et al., 2004). With respect to the regulated endocytosis, in our hands longer incubation periods consistently provided qualitatively comparable results, although they probably underestimate the actual extent of the regulated endocytosis (see table SI).

To test whether our use of a recombinant expression system did not taint our findings, we performed this assay on native, endogenous GluR2 containing AMPARs. Fig. 2C shows a NMDAR-dependent endocytosis of GluR2 essentially as we had found for the recombinant subunits, and in line with published observations (Lee et al., 2004).

NR2B- but not NR2A- containing NMDARs control GluR2-AMPAR endocytosis.

NMDAR-induced changes in AMPAR membrane density are likely to reflect the direction of NMDAR-induced synaptic plasticity. We tested here the hypothesis that NR2B subunits may selectively link NMDAR activation with the endocytosis of GluR2-containing AMPARs. Therefore we used NR2B-selective antagonists, namely ifenprodil (IFP; Williams, 1993) and Ro25-6981 (Ro; Fischer et al., 1997), and the NR2A-preferring antagonist NVP-AAM077 (NVP; Liu et al., 2004; Weitlauf et al., 2005) to investigate the involvement of the NR2B- and NR2A-containing NMDARs in the control of E-GluR2-S endocytosis.

First, we determined the fractional whole-cell currents elicited by NMDA in the presence of NR2 subtype-selective antagonists. The NR2B-selective antagonist IFP inhibited the NMDA-induced currents by approximatively 25% whereas the NR2A-preferring antagonist NVP reduced currents by approximatively 63% (IFP: 75.3 ± 5.17 %, NVP: 36.9 ± 6.79 % of the

Molecular Pharmacology Fast Forward. Published on January 25, 2006 as DOI: 10.1124/mol.105.018580
This article has not been copyedited and formatted. The final version may differ from this version.

test responses, Fig. 3 A). While NVP is a potent antagonist for NR2A-containing NMDARs (Auberson et al., 2002; Liu et al., 2004; Massey et al., 2004) its specificity for NR2A and kinetics has been challenged recently (Berberich et al., 2005; Weitlauf et al., 2005). The findings of Berberich et al. (2005) and of Weitlauf et al. (2005) confirmed that NVP is an efficient NR2A antagonist under the conditions that we have used, i.e. presence of 1µM NVP before and during agonist application, and when steady-state responses were measured. Under these conditions, NVP also produces a 20-30% inhibition of NR2B-containing NMDAR currents.

We have found that NR2B-containing NMDARs carried about 25% of the NMDA-induced whole-cell currents. Therefore, about 5-8 percentage points of the block produced by NVP would represent contaminant NR2B inhibition. The substantially larger block of NMDA-induced currents that we have observed with NVP confirms the existence of NR2A-containing NMDARs in our cultured neurons, in agreement with previously published data (Li et al., 1998).

This demonstrates that both NR2 subunit subtypes are present in our cultures at the stage *in vitro* when the endocytosis experiments were performed. Notably, the NR2B-containing NMDAR subtypes carried only the minority of the NMDAR currents.

When we tested the effect of the NR2 subtype-selective antagonists on AMPAR internalization we observed that both IFP (10 µM) and Ro (1 µM) blocked the NMDAR-induced E-GluR2-S endocytosis (IFP: 1.03 ± 0.23, and Ro: 0.8 ± 0.11, compared to unstimulated controls, see Fig. 3 B, C; raw data are given in Table SI rows 56-65 for IFP, and 66-67 for Ro) as efficiently as the unspecific NMDAR antagonist APV. This by itself suggests a special role for NR2B containing NMDARs in our paradigm. From our electrophysiological data we know that NR2B-containg NMDARs are responsible only for a minority of the NMDA response, whereas the majority is carried by NR2A-containg

Molecular Pharmacology Fast Forward. Published on January 25, 2006 as DOI: 10.1124/mol.105.018580
This article has not been copyedited and formatted. The final version may differ from this version.

NMDARs. Therefore we also tested the effect of NVP, which efficiently blocks the NR2A responses. We observed that NVP (1 μM) did not alter the endocytosis of E-GluR2-S induced by NMDAR activation (Fig. 3 B, C). This effectively rules out NR2A-containing NMDAR as major players in the NMDA-induced GluR2 endocytosis (at least in primary hippocampal neurons). As we have not found any inhibition of NMDA-induced GluR2 endocytosis with NVP, the reduced NR2 subtype specificity of this compound is not relevant in this context. Neither antagonist significantly affected the constitutive endocytosis of E-GluR2-S (Fig. 3 C). These results were reproduced when we used higher agonist concentrations and extended live antibody incubation times (Table SI rows 51, 55, 57, 65-67, 69 and 71).

Our data further suggest that a partial blockage of 20-30% of NR2B-containing NMDAR is not sufficient to block NMDA-induced GluR2 endocytosis.

To test the effect of partial block of NR2B-containing NMDARs we determined the NMDA-induced endocytosis in the presence of concentrations of IFP at and below its IC50 for NR2B (Williams, 1993; Williams et al., 1993). Fig. S4 and Table SI rows 58-62 indeed show that as predicted, such low concentrations of IFP did not inhibit the NMDAR-regulated endocytosis.

Furthermore, experiments on the native endogenous GluR2 receptors revealed the same NR2 subtype dependency (Fig 3D and Table SI rows 87-91). Taken together, our findings reveal that the NMDA-induced GluR2 endocytosis is selectively enhanced by NR2B-containing NMDARs.

NMDARs with Ca^{2+} impermeable channels cannot control AMPAR endocytosis.

To test for the role of the NMDAR-carried Ca^{2+} influx in the endocytosis of AMPARs without contributions from the voltage-gated Ca^{2+} channels, we activated NMDARs in the absence of extracellular Na^+ ions (0 mM $[Na^+]_o$). This protocol allows only Ca^{2+} ions to enter through the NMDAR channel while reducing the depolarizing effects of the Na^+ ions which

Molecular Pharmacology Fast Forward. Published on January 25, 2006 as DOI: 10.1124/mol.105.018580
This article has not been copyedited and formatted. The final version may differ from this version.

are the main charge carriers of NMDAR currents (Burnashev et al., 1995). Activation of NMDARs under 0 mM $[Na^+]_o$ effectively increased the internalization of E-GluR2-S, comparable to the extent observed in 126 mM extracellular Na^+ (Fig. 4 A and Table SI rows 75-82).

To further address the role of the Ca^{2+} influx through the activated NMDAR channels in the regulation of membrane AMPAR removal, we determined the NMDA-induced intracellular accumulation of E-GluR2-S in cultured hippocampal neurons from mice expressing a mutant NMDAR which is impermeable to Ca^{2+} ions yet is able to undergo agonist-dependent activation (*Grin*$1^{N598R/-}$ mice, Rudhard et al., 2003). In *Grin*$1^{N598R/-}$ mice the NMDA-induced whole-cell currents are comparable to those in wild-type littermates. Membrane fraction levels of glutamate receptor subunits, particularly of NR1, NR2A and NR2B (Rudhard et al., 2003) and the membrane targeting of NMDAR subunits (data not shown), are also similar to those in wild-type littermates, which suggests that the presence of Ca^{2+}-impermable NMDARs does not have a global effect on the overall receptor complement.

NMDAR activation in *Grin*$1^{N598R/-}$ neurons failed to enhance the E-GluR2-S endocytosis (1.09 ± 0.16 normalized to unstimulated *Grin*$1^{N598R/-}$ neurons, Fig. 4 B and Table SI rows 72, 73). This observation is in line with the experiments with wild-type neurons in 0 mM $[Na^+]_o$ and indicates that the fractional Ca^{2+} currents carried by the NMDAR channels are necessary and sufficient to induce E-GluR2-S endocytosis. The absolute level of constitutive (i.e., unstimulated) E-GluR2-S internalization determined at 60 min after anti-GFP labeling in *Grin*$1^{N598R/-}$ neurons was 0.4 ± 0.06 (1.92 ± 0.3 times the unstimulated endocytosis in wild-type neurons, Table SI rows 8 and 72). We observed a comparably high level of unstimulated E-GluR2-S endocytosis in neurons from NR1 knockout mice as well (internalized fraction: 0.5 ± 0.05, n=21, $p<0.001$ compared to unstimulated wild-type cells, Table SI row 74). Given the importance of NMDARs in the tonic regulation of AMPAR trafficking (Zhu et al., 2005),

Molecular Pharmacology Fast Forward. Published on January 25, 2006 as DOI: 10.1124/mol.105.018580
This article has not been copyedited and formatted. The final version may differ from this version.

it would be expected that the chronic functional loss generated by the lack of NMDAR-carried Ca^{2+} influx, common to both *Grin*1$^{N598R/-}$ and NR1 knockout genotypes, may have altered the tonic levels of AMPAR internalization and turnover.

Taken together, these results indicate that NMDAR-induced enhancement of GluR2-AMPAR endocytosis requires a Ca^{2+} influx directly through the NMDAR channel, in spite of it representing a minor fraction of the NMDAR current. Considering the earlier observations by Beattie et al. (2000), it appears that in this paradigm, other sources of postsynaptic Ca^{2+} rise activated secondary to membrane depolarization cannot substitute for the NMDAR-generated Ca^{2+} signal.

NMDAR activation enhances the intracellular accumulation of short but not long C-terminal splice variant of E-GluR2.

The interaction domains on the cytoplasmic domains of GluR2 have been previously studied through structure-function analysis (Collingridge et al., 2004). To address the functional role of the native cytoplasmic domain of the GluR2 C-terminal splice variants in the NMDAR-induced removal from the membrane, we expressed E-GluR2-S or EGFP-tagged long C-terminal splice variant (E-GluR2-L) in *Gria*2$^{-/-}$ mice.

In contrast to the E-GluR2-S splice variant NMDA did not enhance the endocytosis of the E-GluR2-L in *Gria*2$^{-/-}$ neurons at any time point studied (Fig. 5A and Table SI rows 29-48). The same GluR2 splice variant dependency was observed on cultures from wild-type *Gria*2$^{+/+}$ mice (Fig. 5C and Table SI rows 3-14, and 21-28).

This indicates that in our paradigm, only the short but not the long C-terminal splice variant is subject to NMDAR-controlled endocytosis, which holds true in regardless of the presence of endogenous GluR2 subunits.

Molecular Pharmacology Fast Forward. Published on January 25, 2006 as DOI: 10.1124/mol.105.018580
This article has not been copyedited and formatted. The final version may differ from this version.

Discussion

The NMDAR-dependent modulation of AMPAR membrane trafficking is an important molecular mechanism in forms of synaptic plasticity where NMDAR activation results in changes of AMPAR membrane density that parallel the changes in synaptic strength (Malenka and Bear, 2004).

To investigate the NMDAR-dependent endocytosis of AMPARs, we expressed N-terminally EGFP-tagged GluR2 subunits (short C-terminal splice variant, E-GluR2-S) in primary hippocampal neurons and determined the NMDA-induced internalization of E-GluR2-S-containing AMPARs with an immunofluorescence-based assay. Although overexpressed individual GluR subunits tend to form homomeric receptors (Shi et al., 2001), our electrophysiological data indicate that E-GluR2-S was incorporated in heteromeric GluR1/E-GluR2-S receptors when expressed in GluR2 knock out background. Furthermore, we observed little difference between the NMDA-induced E-GluR2-S internalization in *Gria*$2^{-/-}$ and wild-type neurons (see Table SI and Figure S3A) suggesting that the GluR2 subunit is functionally dominant in the NMDAR-regulated endocytosis of AMPARs, in line with the observations of Lee et al. (2004).

NMDAR-controlled internalization of GluR2 C-terminal splice variants.

The GluR2 subunit exists in two C-terminal splice variants, whose expression levels are developmentally regulated. The long C-terminal splice variant (GluR2-L) is mostly expressed during the first two postnatal weeks before being overtaken by the short variant and it contributes to the activity-dependent tonic regulation of synaptic AMPARs trafficking (Kolleker et al., 2003; Zhu et al., 2005). The cytoplasmic domain of GluR2-L is homologous to those of GluR1 and GluR4 (Kohler et al., 1994) and lacks the interaction domains of the short GluR2 C-terminus that are involved in NMDAR-dependent internalization of AMPARs (Collingridge et al., 2004). To address the functional role of the long C-terminal GluR2 splice

Molecular Pharmacology Fast Forward. Published on January 25, 2006 as DOI: 10.1124/mol.105.018580
This article has not been copyedited and formatted. The final version may differ from this version.

variant in the NMDAR-regulated AMPAR internalization we expressed a recombinant EGFP-tagged long C-terminal splice variant of GluR2 (E-GluR2-L) in *Gria2*$^{-/-}$ neurons.

We found that NMDAR activation failed to enhance the internalization of E-GluR2-L in *Gria2*$^{-/-}$ neurons, whereas the constitutive level of E-GluR2-L internalization was lower compared to that of the short variant of GluR2. Our observations, together with those of Kolleker et al. (2003), indicate that the developmental transition from GluR2-L expression to the short C-terminal splice variant of GluR2 may substantially affect the NMDAR-dependent targeting and recycling of synaptic AMPARs in hippocampal pyramidal cells *in vivo*.

Specific role of NR2B-containing NMDAR subtypes in GluR2 endocytosis.

In our paradigm, activation of NMDAR signaling independent of the NMDAR subtype resulted in an increased internalization of GluR2 AMPARs *in vitro*, in agreement with previous observations (Lee et al., 2004).

We hypothesized that under our experimental conditions, activation of NR2B-containing NMDAR subtypes triggers selective signaling that leads to the endocytosis of GluR2-containing AMPARs. We tested this hypothesis by means of a pharmacological block directed at the NR2 subunit subtypes. For a discussion on the selectivity of the NR2 subtype antagonists that we used, see the Results section.

Selective inhibition of NR2B-containing NMDARs blocked the NMDA-induced intracellular accumulation of E-GluR2-S, whereas the preferential inhibition of NR2A-containing NMDARs did not have any effect, in line with our hypothesis. Our findings therefore provide direct evidence for a NR2B subtype-specific link between the activation of NMDARs and the downstream signaling leading to GluR2-AMPAR endocytosis.

NR2A and NR2B subunits are widely expressed in the CNS and are considered the major NR2 subunits in the hippocampus, where their expression is developmentally regulated (Kew

Molecular Pharmacology Fast Forward. Published on January 25, 2006 as DOI: 10.1124/mol.105.018580
This article has not been copyedited and formatted. The final version may differ from this version.

et al., 1998; Monyer et al., 1994). At the developmental stage of our cultures, hippocampal neurons express a heterogeneous population of NMDARs, largely formed by NR1/NR2A, NR1/NR2B and NR1/NR2A/NR2B subtypes, paralleling the developmental profile *in vivo* (Kew et al., 1998; Li et al., 2002; Luo et al., 1997). NR2B-containing NMDAR subtypes are both extrasynaptic (largely NR1/NR2B) and synaptic, where they contribute to the heterogenous population of NR1/NR2A and NR1/NR2B diheteromers, along with triheteromeric NR1/NR2A/NR2B (Li et al., 2002; Massey et al., 2004; Tovar and Westbrook, 1999). In our cultures, we found that the whole-cell NMDAR current is carried mainly by NR1/NR2A subtypes, and to a lesser extent by NR2B-containing receptors. At the concentration used in our experiments (10 μM), ifenprodil is thought to inhibit both NR1/NR2B and NR1/NR2A/NR2B heteromers (Kew et al., 1998), but not NR1/NR2A diheteromers (Williams, 1993). In lack of a selective antagonist for triheteromeric NMDARs, it is tempting to speculate that the mere presence of NR2B subunits in the NMDAR complex, regardless of the co-assembly with NR2A, or of a synaptic vs. extrasynaptic location, is sufficient to drive the NMDAR signaling towards the internalization of GluR2-containing AMPARs.

As suggested by the findings of Liu et al. (2004) and of Massey et al. (2004), NR2B-containing NMDARs play a special role in the down-modulation of the synaptic strength. The activation of NMDARs achieved in our experimental paradigm is on a time scale larger than what is usually obtained by electrically induced synaptic activity (e.g., low frequency stimulation protocols). Taking this into account, our findings are likely to reflect an NR2B-selective contribution to mechanisms of global modulation of synaptic strength alike to synaptic scaling (Turrigiano and Nelson, 2004), or to a more local, Hebbian-type modulation such as LTD.

Molecular Pharmacology Fast Forward. Published on January 25, 2006 as DOI: 10.1124/mol.105.018580
This article has not been copyedited and formatted. The final version may differ from this version.

The role of Ca^{2+} influx carried by NMDAR channels in the regulated endocytosis of AMPARs.

Similar to NMDAR-dependent LTD, a transient increase of the postsynaptic Ca^{2+} concentration following glutamate receptor activation is required for the regulated internalization of AMPARs and operates at multiple levels, including the clathrin-mediated endocytosis (Collingridge et al., 2004). However, the exact role of the Ca^{2+} influx carried by the NMDAR channels in the signaling pathway leading to AMPAR endocytosis is still elusive.

We observed that the removal of extracellular Na^{+} does not alter the capability of activated NMDARs to enhance E-GluR2-S internalization, which suggests that depolarization-dependent Ca^{2+} sources are not essential for this effect, in line with earlier observations (Beattie et al., 2000). Furthermore, activation of Ca^{2+}-impermeable NMDARs in *Grin*$1^{N598R/-}$ mice failed to enhance the intracellular accumulation of E-GluR2-S. Together, these results provide direct evidence that Ca^{2+} influx through the activated NMDAR channels (and not from other sources) mediates the NMDAR-dependent signaling cascade for the induction of GluR2 AMPAR endocytosis.

A very likely explanation of our finding is that a Ca^{2+} signal localized at the NMDAR-associated complex is the initiating signaling step in this regulated GluR2 AMPARs internalization. Such Ca^{2+} nanodomain signals (reviewed in Augustine et al., 2003) rely on Ca^{2+} "sensors" located in close proximity to the Ca^{2+} source. The morphological and biochemical correlate of such nanodomains could well be the NMDAR-associated complex as defined by proteomic analysis (Husi et al., 2000).

In conclusion, we have shown that the NMDAR-regulated removal of membrane AMPARs containing the short C-terminal splice variant of GluR2 specifically involves NR2B-containing NMDAR subtypes and relies critically on the Ca^{2+} influx carried through NMDARs (Fig. 6). Recent observations by Kim et al. (2005) and Zhu et al. (2005) support the

Molecular Pharmacology Fast Forward. Published on January 25, 2006 as DOI: 10.1124/mol.105.018580
This article has not been copyedited and formatted. The final version may differ from this version.

model that different NMDAR subtypes employ different signaling pathways for the modulation of AMPAR trafficking. Our findings suggest that the link between the subunit composition of NMDARs and the selective activation of these pathways may be provided by the highly localized, NR2 subtype-specific processing of the NMDAR-carried Ca^{2+} signal.

Molecular Pharmacology Fast Forward. Published on January 25, 2006 as DOI: 10.1124/mol.105.018580
This article has not been copyedited and formatted. The final version may differ from this version.

Acknowledgements

We thank Drs. P. Osten and S. Schlesinger for Sindbis vectors.

Molecular Pharmacology Fast Forward. Published on January 25, 2006 as DOI: 10.1124/mol.105.018580
This article has not been copyedited and formatted. The final version may differ from this version.

References

Auberson YP, Allgeier H, Bischoff S, Lingenhoehl K, Moretti R and Schmutz M (2002) 5-Phosphonomethylquinoxalinediones as competitive NMDA receptor antagonists with a preference for the human 1A/2A, rather than 1A/2B receptor composition. *Bioorg Med Chem Lett* **12**:1099-102.

Augustine GJ, Santamaria F and Tanaka K (2003) Local calcium signaling in neurons. *Neuron* **40**:331-46.

Beattie EC, Carroll RC, Yu X, Morishita W, Yasuda H, von Zastrow M and Malenka RC (2000) Regulation of AMPA receptor endocytosis by a signaling mechanism shared with LTD. *Nat Neurosci* **3**:1291-300.

Berberich S, Punnakkal P, Jensen V, Pawlak V, Seeburg PH, Hvalby O and Kohr G (2005) Lack of NMDA receptor subtype selectivity for hippocampal long-term potentiation. *J Neurosci* **25**:6907-10.

Burnashev N, Zhou Z, Neher E and Sakmann B (1995) Fractional calcium currents through recombinant GluR channels of the NMDA, AMPA and kainate receptor subtypes. *J Physiol* **485 (Pt 2)**:403-18.

Collingridge GL, Isaac JT and Wang YT (2004) Receptor trafficking and synaptic plasticity. *Nat Rev Neurosci* **5**:952-62.

Dingledine R, Borges K, Bowie D and Traynelis SF (1999) The glutamate receptor ion channels. *Pharmacol Rev* **51**:7-61.

Fischer G, Mutel V, Trube G, Malherbe P, Kew JN, Mohacsi E, Heitz MP and Kemp JA (1997) Ro 25-6981, a highly potent and selective blocker of N-methyl-D-aspartate receptors containing the NR2B subunit. Characterization in vitro. *J Pharmacol Exp Ther* **283**:1285-92.

Hayashi Y, Shi SH, Esteban JA, Piccini A, Poncer JC and Malinow R (2000) Driving AMPA receptors into synapses by LTP and CaMKII: requirement for GluR1 and PDZ domain interaction. *Science* **287**:2262-7.

Husi H, Ward MA, Choudhary JS, Blackstock WP and Grant SG (2000) Proteomic analysis of NMDA receptor-adhesion protein signaling complexes. *Nat Neurosci* **3**:661-9.

Jia Z, Agopyan N, Miu P, Xiong Z, Henderson J, Gerlai R, Taverna FA, Velumian A, MacDonald J, Carlen P, Abramow-Newerly W and Roder J (1996) Enhanced LTP in mice deficient in the AMPA receptor GluR2. *Neuron* **17**:945-56.

Keinanen K, Wisden W, Sommer B, Werner P, Herb A, Verdoorn TA, Sakmann B and Seeburg PH (1990) A family of AMPA-selective glutamate receptors. *Science* **249**:556-60.

Kew JN, Richards JG, Mutel V and Kemp JA (1998) Developmental changes in NMDA receptor glycine affinity and ifenprodil sensitivity reveal three distinct populations of NMDA receptors in individual rat cortical neurons. *J Neurosci* **18**:1935-43.

Kim J, Dittgen T, Nimmerjahn A, Waters J, Pawlak V, Helmchen F, Schlesinger S, Seeburg PH and Osten P (2004) Sindbis vector SINrep(nsP2S726): a tool for rapid heterologous expression with attenuated cytotoxicity in neurons. *J Neurosci Methods* **133**:81-90.

Kim MJ, Dunah AW, Wang YT and Sheng M (2005) Differential Roles of NR2A- and NR2B-Containing NMDA Receptors in Ras-ERK Signaling and AMPA Receptor Trafficking. *Neuron* **46**:745-60.

Kohler M, Kornau HC and Seeburg PH (1994) The organization of the gene for the functionally dominant alpha-amino-3-hydroxy-5-methylisoxazole-4-propionic acid receptor subunit GluR-B. *J Biol Chem* **269**:17367-70.

Kolleker A, Zhu JJ, Schupp BJ, Qin Y, Mack V, Borchardt T, Kohr G, Malinow R, Seeburg PH and Osten P (2003) Glutamatergic plasticity by synaptic delivery of GluR-B(long)-containing AMPA receptors. *Neuron* **40**:1199-212.

Lee SH, Simonetta A and Sheng M (2004) Subunit rules governing the sorting of internalized AMPA receptors in hippocampal neurons. *Neuron* **43**:221-36.

Li B, Chen N, Luo T, Otsu Y, Murphy TH and Raymond LA (2002) Differential regulation of synaptic and extra-synaptic NMDA receptors. *Nat Neurosci* **5**:833-4.

Li JH, Wang YH, Wolfe BB, Krueger KE, Corsi L, Stocca G and Vicini S (1998) Developmental changes in localization of NMDA receptor subunits in primary cultures of cortical neurons. *Eur J Neurosci* **10**:1704-15.

Lisman J (1989) A mechanism for the Hebb and the anti-Hebb processes underlying learning and memory. *Proc Natl Acad Sci U S A* **86**:9574-8.

Liu L, Wong TP, Pozza MF, Lingenhoehl K, Wang Y, Sheng M, Auberson YP and Wang YT (2004) Role of NMDA receptor subtypes in governing the direction of hippocampal synaptic plasticity. *Science* **304**:1021-4.

Luo J, Wang Y, Yasuda RP, Dunah AW and Wolfe BB (1997) The majority of N-methyl-D-aspartate receptor complexes in adult rat cerebral cortex contain at least three different subunits (NR1/NR2A/NR2B). *Mol Pharmacol* **51**:79-86.

Malenka RC and Bear MF (2004) LTP and LTD: an embarrassment of riches. *Neuron* **44**:5-21.

Massey PV, Johnson BE, Moult PR, Auberson YP, Brown MW, Molnar E, Collingridge GL and Bashir ZI (2004) Differential roles of NR2A and NR2B-containing NMDA receptors in cortical long-term potentiation and long-term depression. *J Neurosci* **24**:7821-8.

Monyer H, Burnashev N, Laurie DJ, Sakmann B and Seeburg PH (1994) Developmental and regional expression in the rat brain and functional properties of four NMDA receptors. *Neuron* **12**:529-40.

Rudhard Y, Kneussel M, Nassar MA, Rast GF, Annala AJ, Chen PE, Tigaret CM, Dean I, Roes J, Gibb AJ, Hunt SP and Schoepfer R (2003) Absence of Whisker-related pattern formation in mice with NMDA receptors lacking coincidence detection properties and calcium signaling. *J Neurosci* **23**:2323-32.

Sheng M and Kim MJ (2002) Postsynaptic signaling and plasticity mechanisms. *Science* **298**:776-80.

Shi S, Hayashi Y, Esteban JA and Malinow R (2001) Subunit-specific rules governing AMPA receptor trafficking to synapses in hippocampal pyramidal neurons. *Cell* **105**:331-43.

Shi SH, Hayashi Y, Petralia RS, Zaman SH, Wenthold RJ, Svoboda K and Malinow R (1999) Rapid spine delivery and redistribution of AMPA receptors after synaptic NMDA receptor activation. *Science* **284**:1811-6.

Specht CG, Tigaret CM, Rast GF, Thalhammer A, Rudhard Y and Schoepfer R (2005) Subcellular localisation of recombinant alpha- and gamma-synuclein. *Mol Cell Neurosci* **28**:326-34.

Tovar KR and Westbrook GL (1999) The incorporation of NMDA receptors with a distinct subunit composition at nascent hippocampal synapses in vitro. *J Neurosci* **19**:4180-8.

Turrigiano GG and Nelson SB (2004) Homeostatic plasticity in the developing nervous system. *Nat Rev Neurosci* **5**:97-107.

Weitlauf C, Honse Y, Auberson YP, Mishina M, Lovinger DM and Winder DG (2005) Activation of NR2A-containing NMDA receptors is not obligatory for NMDA receptor-dependent long-term potentiation. *J Neurosci* **25**:8386-90.

Wenthold RJ, Petralia RS, Blahos J, II and Niedzielski AS (1996) Evidence for multiple AMPA receptor complexes in hippocampal CA1/CA2 neurons. *J Neurosci* **16**:1982-9.

Wenthold RJ, Prybylowski K, Standley S, Sans N and Petralia RS (2003) Trafficking of NMDA receptors. *Annu Rev Pharmacol Toxicol* **43**:335-58.

Williams K (1993) Ifenprodil discriminates subtypes of the N-methyl-D-aspartate receptor: selectivity and mechanisms at recombinant heteromeric receptors. *Mol Pharmacol* **44**:851-9.

Williams K, Russell SL, Shen YM and Molinoff PB (1993) Developmental switch in the expression of NMDA receptors occurs in vivo and in vitro. *Neuron* **10**:267-78.

Zhu JJ, Esteban JA, Hayashi Y and Malinow R (2000) Postnatal synaptic potentiation: delivery of GluR4-containing AMPA receptors by spontaneous activity. *Nat Neurosci* **3**:1098-106.

Zhu Y, Pak D, Qin Y, McCormack SG, Kim MJ, Baumgart JP, Velamoor V, Auberson YP, Osten P, van Aelst L, Sheng M and Zhu JJ (2005) Rap2-JNK Removes Synaptic AMPA Receptors during Depotentiation. *Neuron* **46**:905-16.

Molecular Pharmacology Fast Forward. Published on January 25, 2006 as DOI: 10.1124/mol.105.018580
This article has not been copyedited and formatted. The final version may differ from this version.

Footnotes:

*This work was funded by a Wellcome Trust Senior Fellowship and a Wellcome grant to RS, and a BBSRC grant to MS&RS. CMT was supported in part by a Wellcome Trust Traveling Fellowship, and GFR was recipient of a DFG Emma Noether Fellowship.

Person to receive reprint requests: Ralf Schoepfer, Laboratory for Molecular Pharmacology, Department of Pharmacology, UCL, Gower Street, London WC1E 6BT, UK; Tel +44-20-76797242, Fax +44-20-76797245, E-mail: r.schoepfer@ucl.ac.uk

Molecular Pharmacology Fast Forward. Published on January 25, 2006 as DOI: 10.1124/mol.105.018580
This article has not been copyedited and formatted. The final version may differ from this version.

Legends for figures

Figure 1. E-GluR2-S rescues wild-type AMPAR phenotype in Gria2$^{-/-}$ neurons.

A, Left: I-V relationships of 100 µM kainate-evoked whole-cell steady-state currents of cultured hippocampal wild-type neurons (triangles, n=5 cells), naive *Gria*2$^{-/-}$ neurons (squares, n=4) and *Gria*2$^{-/-}$ neurons expressing E-GluR2-S (circles, n=4). Right: representative kainate responses for the individual genotypes at holding membrane potential (Vh) starting at -60 mV in 20 mV increments, horizontal bar indicates kainate application (5 s); scale bars: 100 pA and 2 s. *B,* Rectification indices for the recordings shown in A. Data are means ± SEM of the values normalized to the currents at -60 mV; **p*<0.05.

Figure 2. NMDAR-induced internalization of E-GluR2-S-containg AMPARs.

A, Z axis-projected confocal images of *Gria*2$^{-/-}$ neurons expressing recombinant E-GluR2-S (green in Merged) with anti-GFP immunofluorescence for surface (blue in Merged) and internalized (red in Merged) E-GluR2-S AMPARs 60 min after treatment with aCSF alone (Unstimulated) or agonist (NMDA: 100 µM NMDA + 1 µM Gly). Antibody staining as in Supplementary Table SI rows 33 & 38). Scale bar: 20 µm. *B,* Internalization of E-GluR2-S in wild-type neurons 20 min after stimulation with 20 µM NMDA + 10 µM Gly alone (NMDA: n=15) or in the presence of 50 µM APV (NMDA + APV: n=5) or after 50 µM APV only (APV: n=5). The bars represent mean ± SEM internalized fraction (10 min live antibody incubations) normalized to unstimulated controls (Unstim.: n=19). Raw data are in Table SI rows 6 (Unstim.), 12 (NMDA), 68 (APV), and 70 (NMDA + APV). *C,* Internalization of native, endogenous GluR2-containing AMPARs in wild-type cells, 5 min after treatment as in (B); raw data are in Table SI rows 83 to 86. ***p*<0.01 and ****p*<0.001 compared to unstimulated controls.

Molecular Pharmacology Fast Forward. Published on January 25, 2006 as DOI: 10.1124/mol.105.018580
This article has not been copyedited and formatted. The final version may differ from this version.

Figure 3. NR2B- but not NR2A-containing NMDARs control the internalization of E-GluR2-S.

A, Left: Whole-cell responses to 20 μM NMDA + 10 μM Gly recorded at DIV 15-21 in the presence of 1 μM NVP-AAM077 (NVP: n=11) or 10 μM ifenprodil (IFP: n=9). Right: NMDAR currents in the presence of NVP (top, middle trace) or IFP (bottom, middle), shown between consecutive test NMDA responses. Columns represent mean ± SEM of steady-state current amplitude normalized to the amplitude of the test response before antagonist perfusion; horizontal bars above traces: agonist application (30 s); scale bars: 100 pA, 30 s. *B*, Z axis-projected confocal images of E-GluR2-S internalization assay (pseudo-colors as in Fig. 2) taken from treatment groups in C. Scale bar: 20 μm. *C*, Internalization of E-GluR2-S in wild-type cells 20 min after stimulation with 20 μM NMDA + 10 μM Gly (NMDA: n=15) alone or in the presence of either 10 μM IFP (NMDA+IFP: n=8) or 1 μM NVP (NMDA+NVP: n=24). IFP, NVP: cells treated with antagonist only (n=7, and n=10). Bars represent mean ± SEM of internalized fraction normalized to unstimulated controls (Unstim.: n=19). Raw values are in Table SI rows 6 (Unstim.), 12 (NMDA), 50 (NVP), 56 (IFP), 53 (NMDA+NVP) and 63 (NMDA+IFP). *D*, Internalization of the native, endogenous GluR2 AMPARs, determined 5 min after treatment as in (C); raw data are in Table SI rows 83 (Unstim), 84 (NMDA), 87 (IFP), 89 (NMDA+IFP), 90 (NVP) and 91 (NMDA+NVP). $^{**}p<0.01$, and $^{***}p<0.001$ compared to unstimulated controls..

Molecular Pharmacology Fast Forward. Published on January 25, 2006 as DOI: 10.1124/mol.105.018580
This article has not been copyedited and formatted. The final version may differ from this version.

Figure 4. NMDAR-controlled internalization of E-GluR-S requires Ca^{2+} influx through NMDAR channels.

A, E-GluR2-S internalization in wild-type neurons in the absence of extracellular Na^+ (0 mM $[Na^+]_o$) at 5 min under baseline conditions (Unstim.: n=10) and after stimulation with 20 µM NMDA + 10 µM Gly (NMDA: n=6) or in normal HEPES-Ringer (126 mM $[Na^+]_o$, Unstim.: n=9, NMDA: n=7). Raw data are in Table SI rows 75, 77, 79, and 81, respectively. *B*, Internalization of E-GluR2-S AMPARs in neurons from the indicated genotypes, under baseline conditions (Unstim., wild-type: n=52, Table SI row 8; *Grin*$1^{N598R/-}$: n=12, Table SI row 72) and after NMDAR activation alone (NMDA, wild-type: n = 46, Table SI row 20; *Grin*$1^{N598R/-}$: n=15, Table SI row 73) or in the presence of 100 µM APV (NMDA+APV: n=24, Table SI row 71). In B, internalization was determined with live antibody incubations of 40 min (anti-GFP) and 30 min (Cy5 conjugate), 60 min after treatment. Values are mean ± SEM internalized fraction normalized to unstimulated controls within each group. *p< 0.05, **p<0.01, ***p<0.001, and #p=0.17 between data under the brackets.

Molecular Pharmacology Fast Forward. Published on January 25, 2006 as DOI: 10.1124/mol.105.018580
This article has not been copyedited and formatted. The final version may differ from this version.

Figure 5. NMDAR-induced internalization of E-GluR2-S-containg AMPARs is restricted to the short splice variant.

A, Internalization of E-GluR2-S and E-GluR2-L in *Gria*$2^{-/-}$ neurons, plotted against the time lapsed between stimulation with 20 μM NMDA + 10 μM Gly (NMDA 20) or under baseline conditions (Unstim); raw data are in Table SI rows 29-48. *Insets*: relative internalization at 5 min after stimulation with 20 μM NMDA + 10 μM Gly (NMDA 20, E-GluR2-S n=8, Table SI row 34, E-GluR2-L n=5, Table SI row 44); data are mean ± SEM internalized fraction normalized to the unstimulated control (Unstim, E-GluR2-S: n=10, Table SI row 29; E-GluR2-L: n=6, Table SI row 39). Data for time points 5-30 min were fitted to one-phase exponential association equation, and correlation coefficients were 0.89 (E-GluR2-S Unstim), 0.93 (E-GluR2-S NMDA 20), 0.90 (E-GluR2-L Unstim) and 0.82 (E-GluR2-L NMDA 20). Data for time point 60 were obtained with antibody incubation times of 40 min (anti-GPP) and 30 min for the Cy5 conjugate. $^{**}p<0.01$. *B*, E-GluR2-S-expressing *Gria*$2^{-/-}$ neuron (green) that has been stained for surface (blue) and internalized (red) E-GluR2-S at 5 min under baseline conditions, and for synaptophysin (yellow). Typical regions of close proximity between surface E-GluR2-S and synaptophysin-positive structures are indicated by arrow-heads; the double arrow-head indicates an area where E-GluR2-S internalization has occurred; scale bar: 20 μm. *C*, Internalization of E-GluR2-S and E-GluR2-L in wild-type neurons under conditions identical to insets in A; raw data are in Table SI rows 3, 9, 21 and p25, respectively; $^{**}p<0.01$ and $\#p=0.22$ between data under the brackets.

Figure 6. Scheme of the relation between NMDAR (NR2) subtypes, NMDAR-carried Ca^{2+} *influx and internalization of GluR2-containing AMPAR.*

Ca^{2+} permeation through activated NR2B-, but not NR2A-containing NMDARs, is necessary for the NMDAR-dependent endocytosis of AMPARs that incorporate the short, but not long, C-terminal splice variant of GluR2.

Molecular Pharmacology Fast Forward. Published on January 25, 2006 as DOI: 10.1124/mol.105.018580
This article has not been copyedited and formatted. The final version may differ from this version.

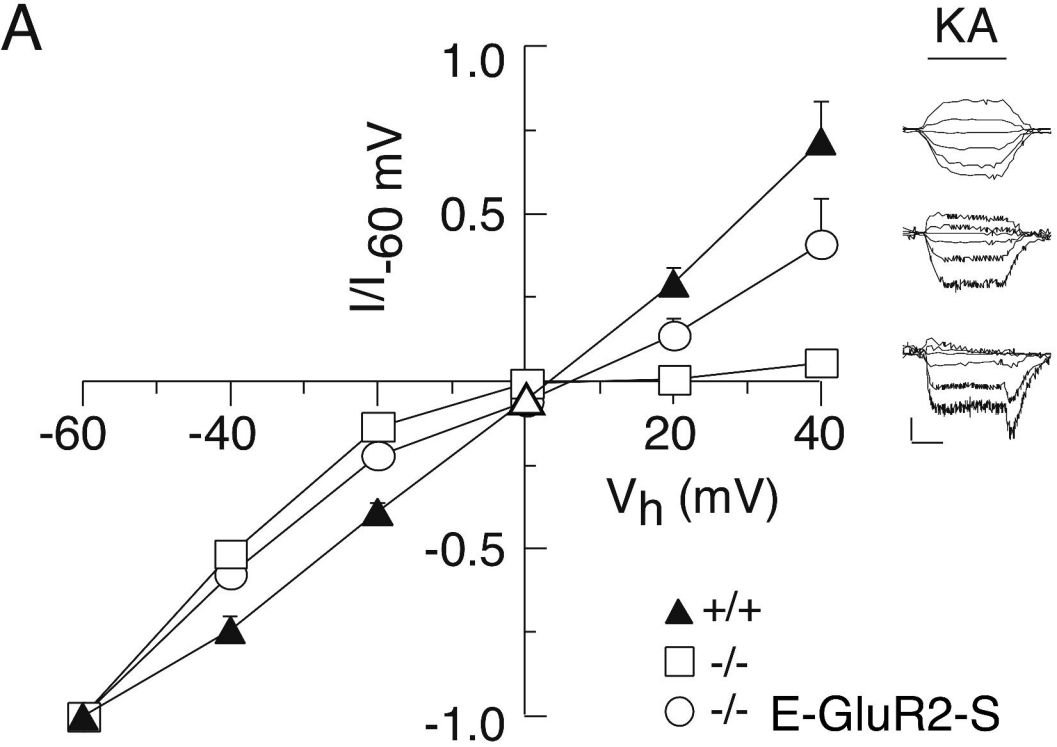

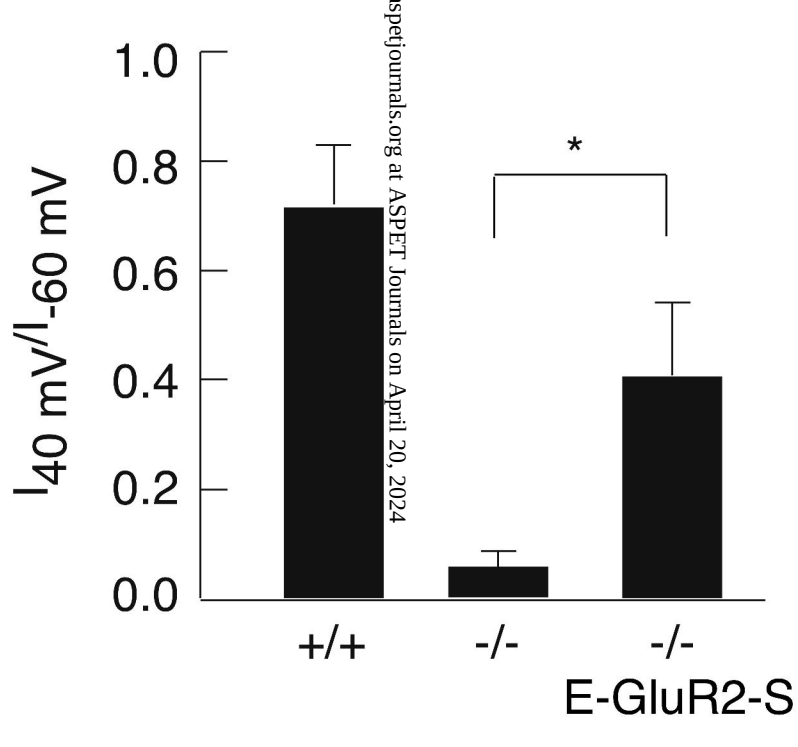

Figure 1

A

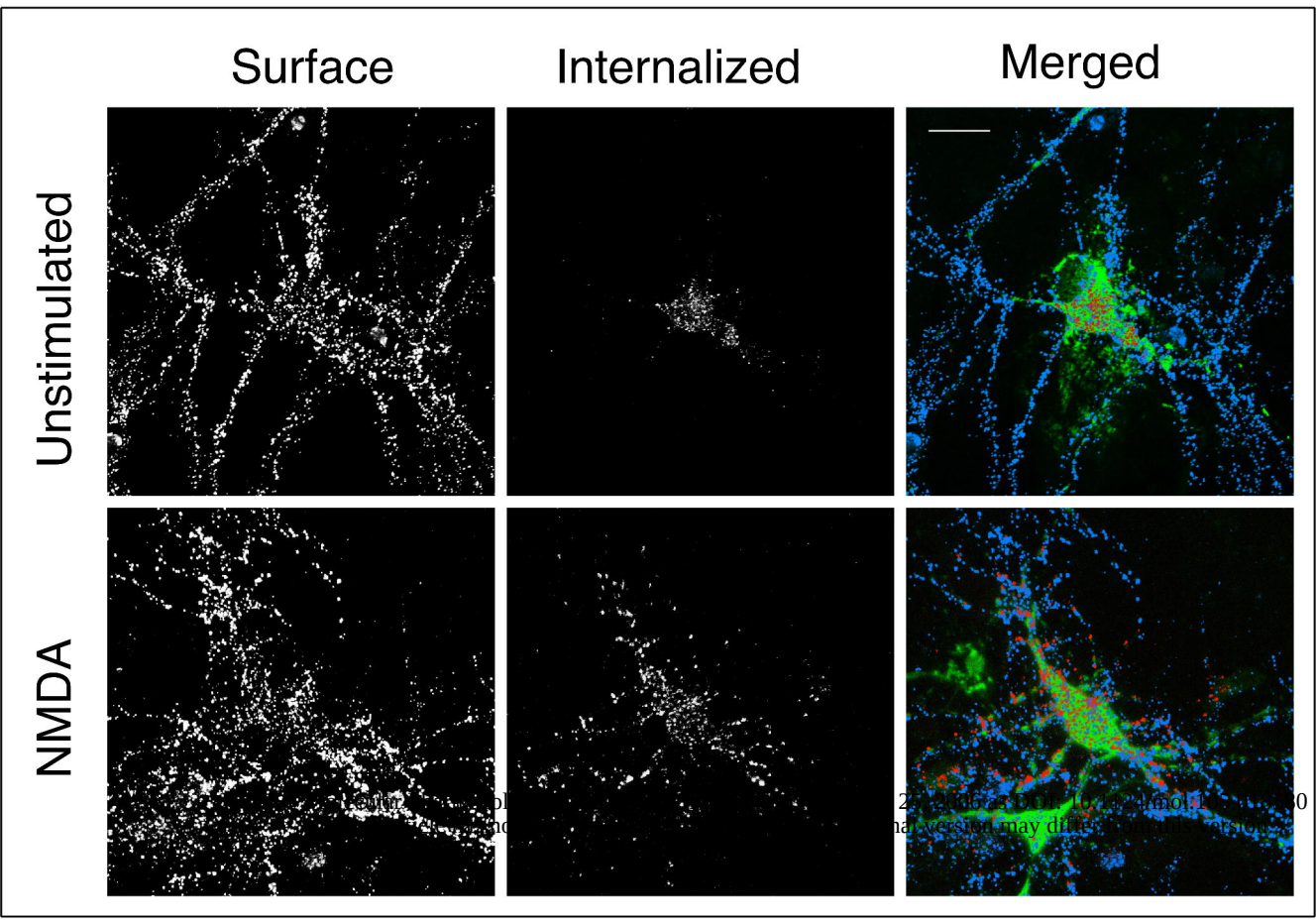
Surface
Internalized
Merged
Unstimulated
NMDA

B

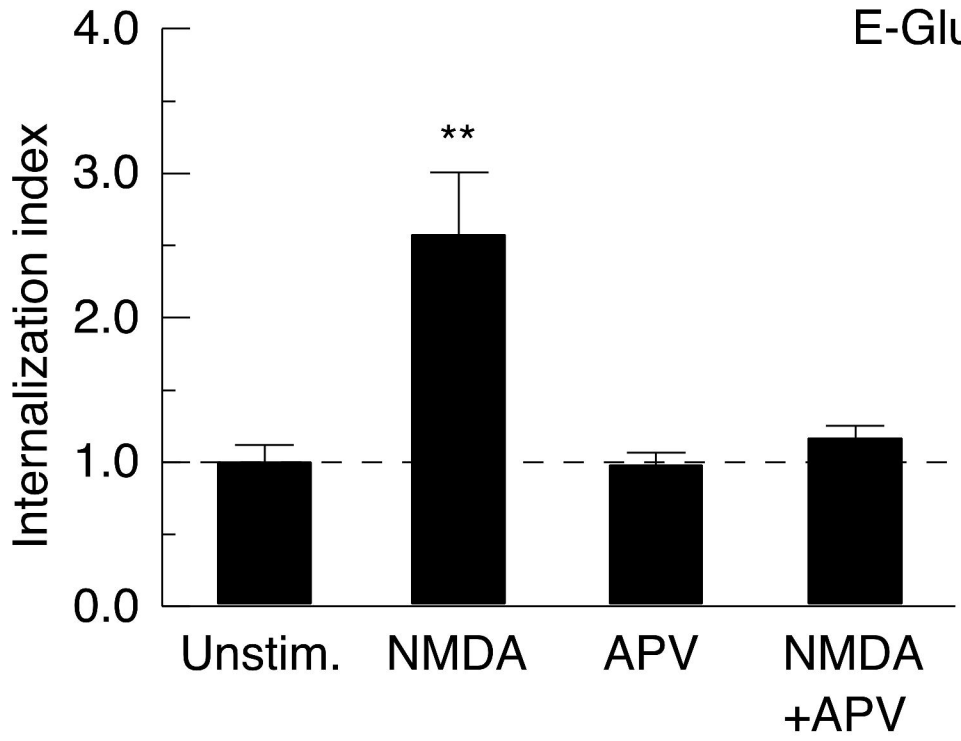
E-GluR2-S
Internalization index
4.0
3.0
2.0
1.0
0.0
**
Unstim.
NMDA
APV
NMDA
+APV

C

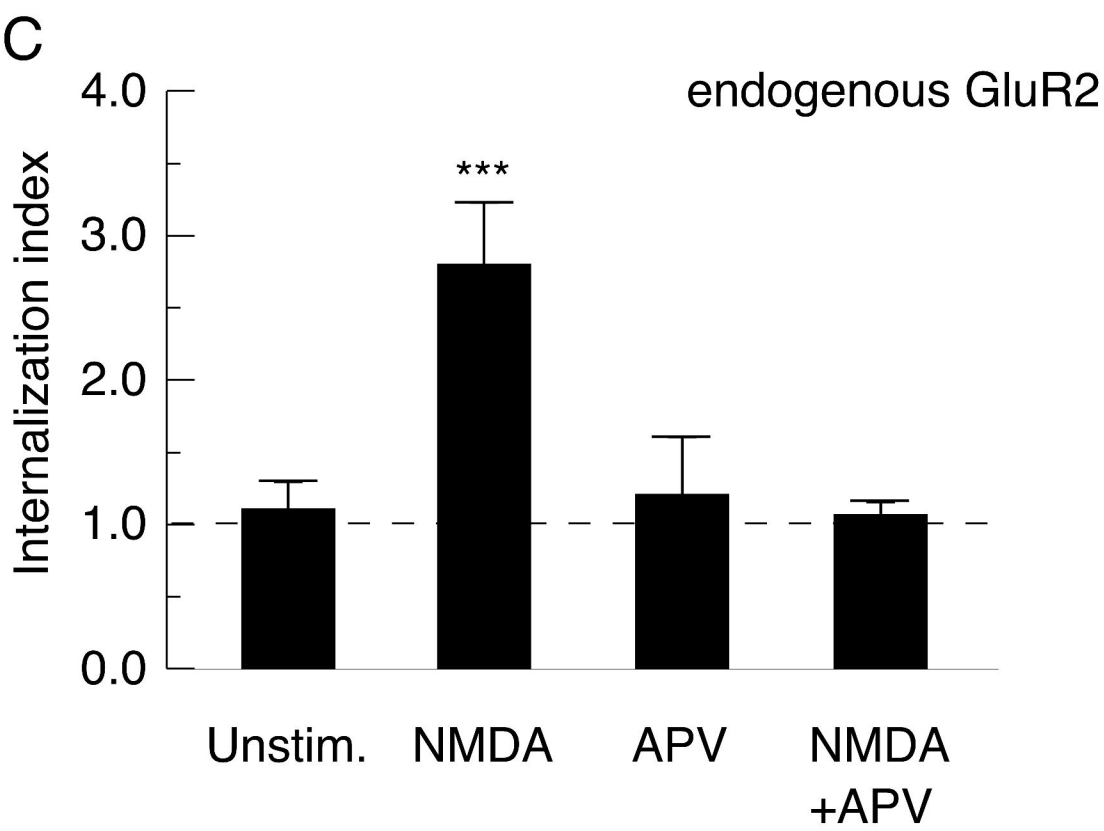
endogenous GluR2
Internalization index
4.0
3.0
2.0
1.0
0.0
***
Unstim.
NMDA
APV
NMDA
+APV

Figure 2

A

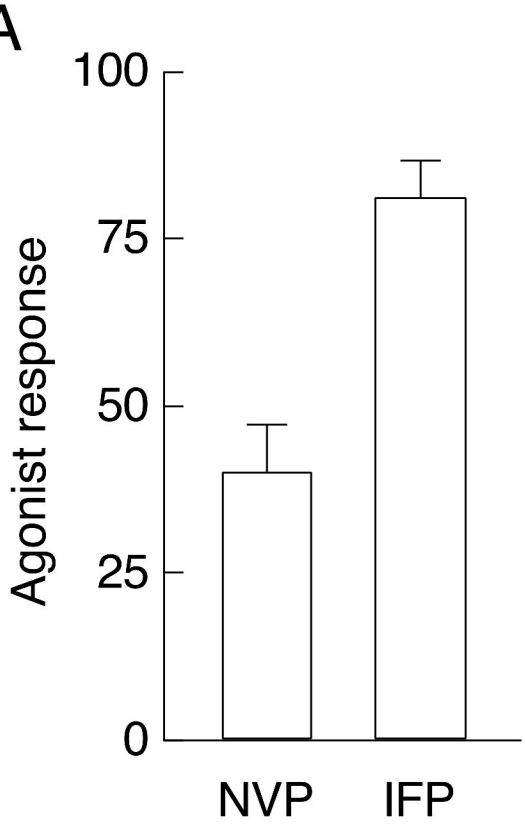
100
75
50
25
0
Agonist response
NVP
IFP

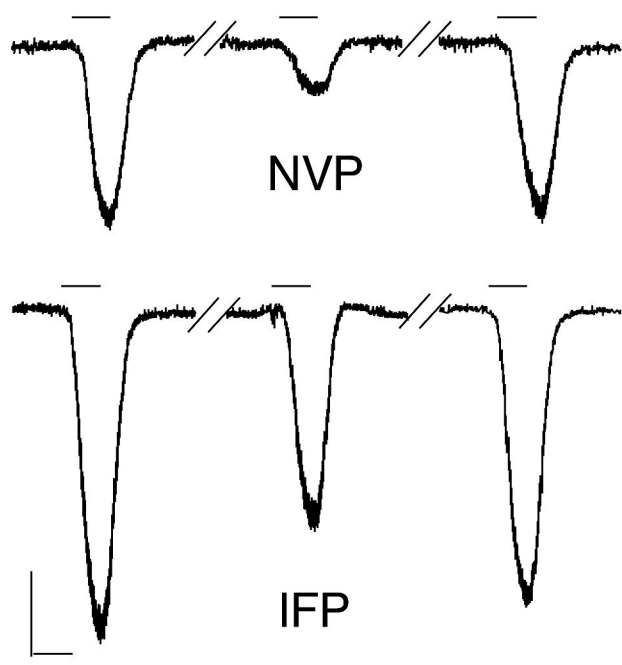
NVP
IFP

B

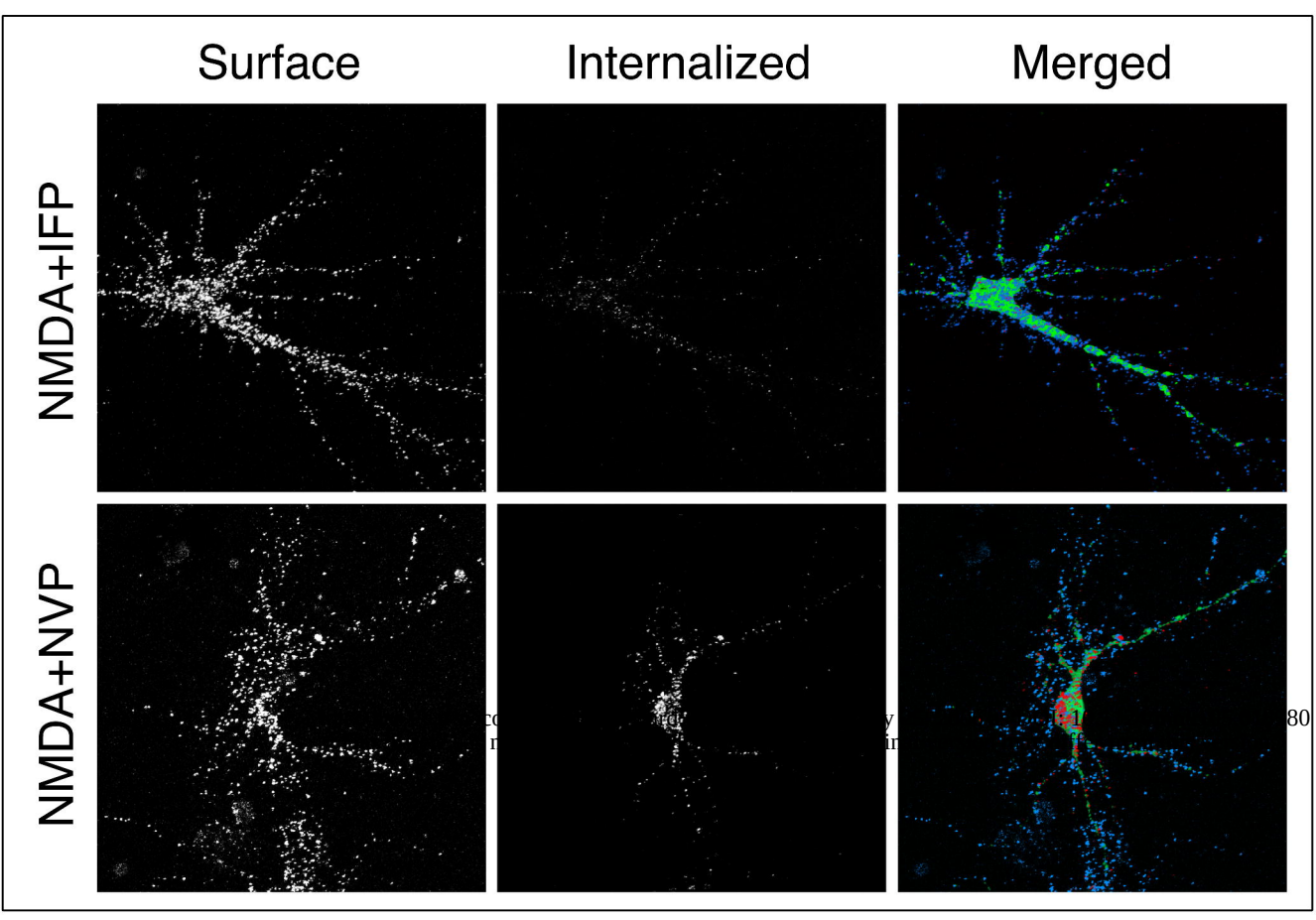
Surface
Internalized
Merged
NMDA+IFP
NMDA+NVP

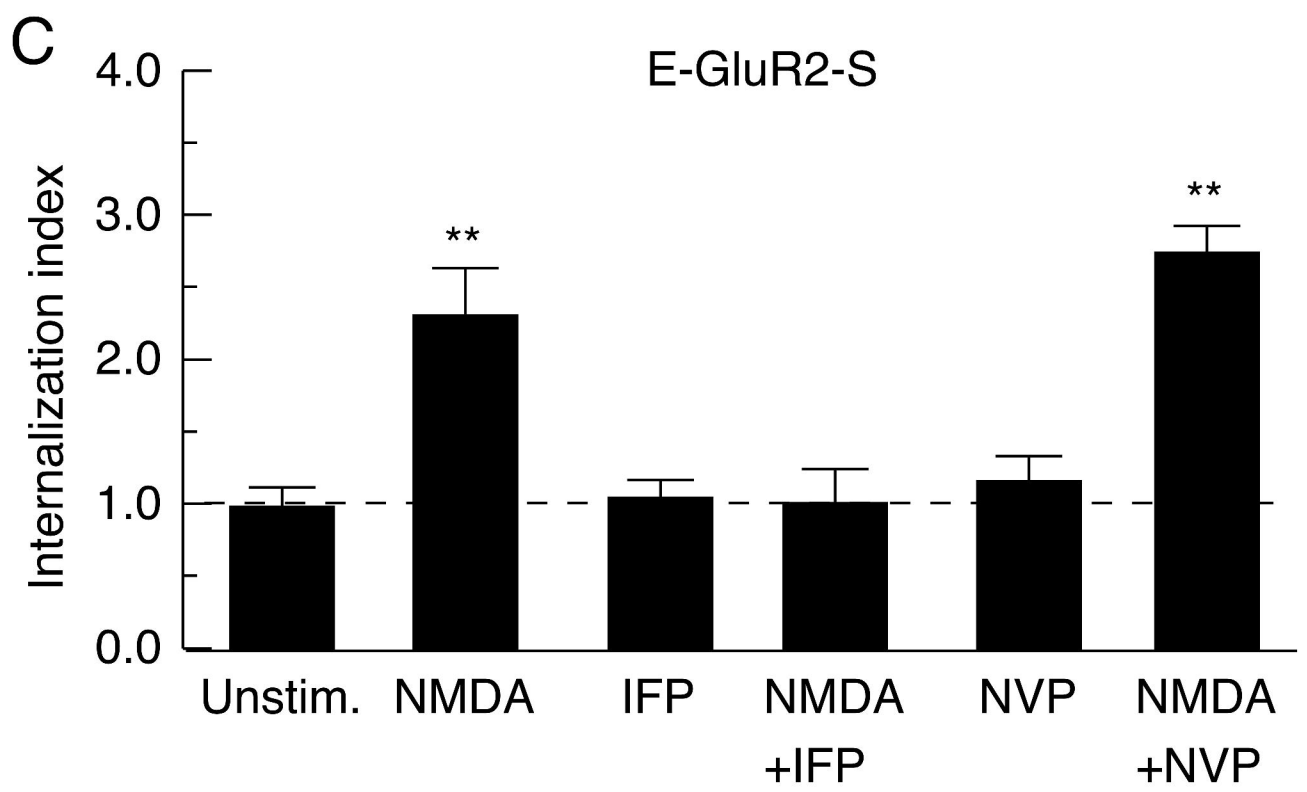
C
E-GluR2-S
Internalization index
4.0
3.0
2.0
1.0
0.0
**
**
Unstim.
NMDA
IFP
NMDA +IFP
NVP
NMDA +NVP

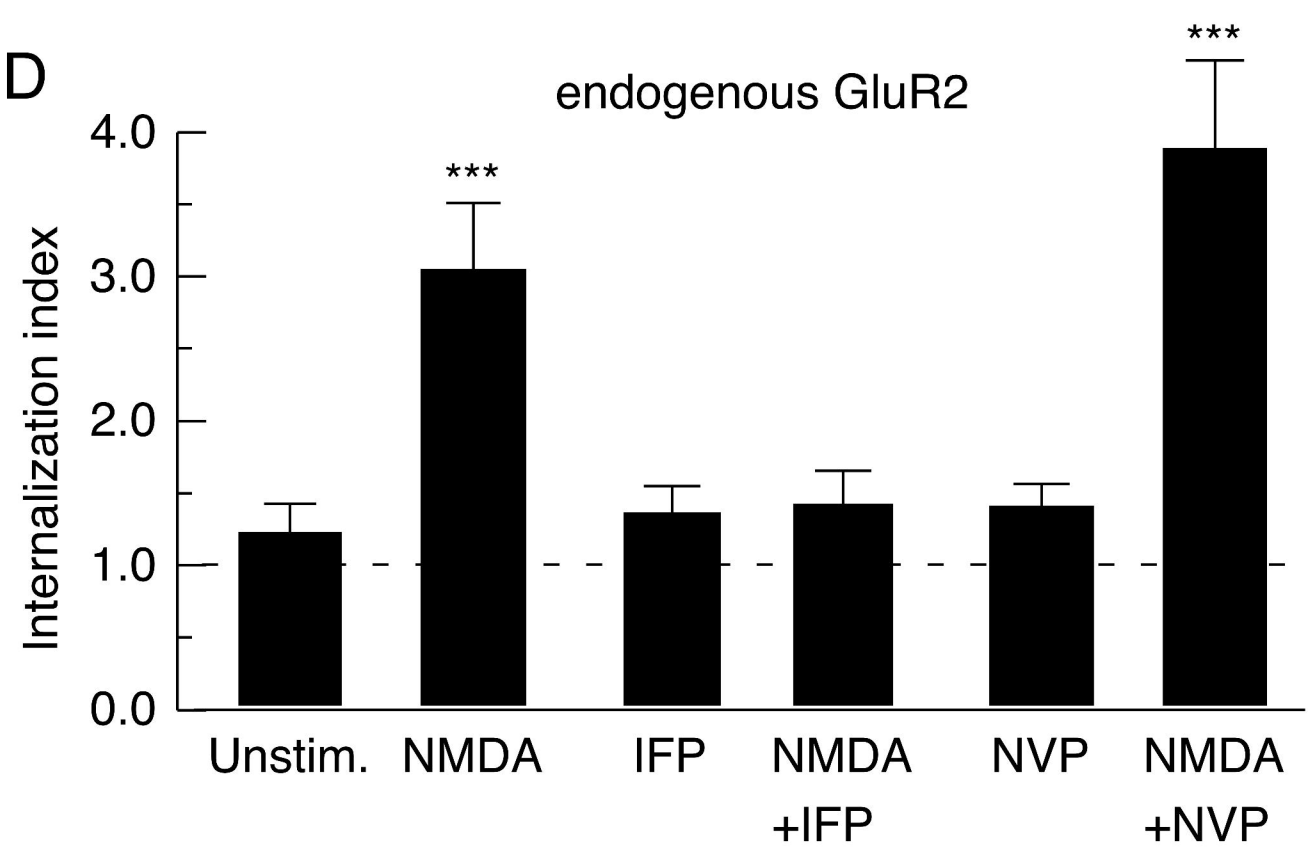
D
endogenous GluR2
Internalization index
4.0
3.0
2.0
1.0
0.0
***
***
Unstim.
NMDA
IFP
NMDA +IFP
NVP
NMDA +NVP

Figure 3

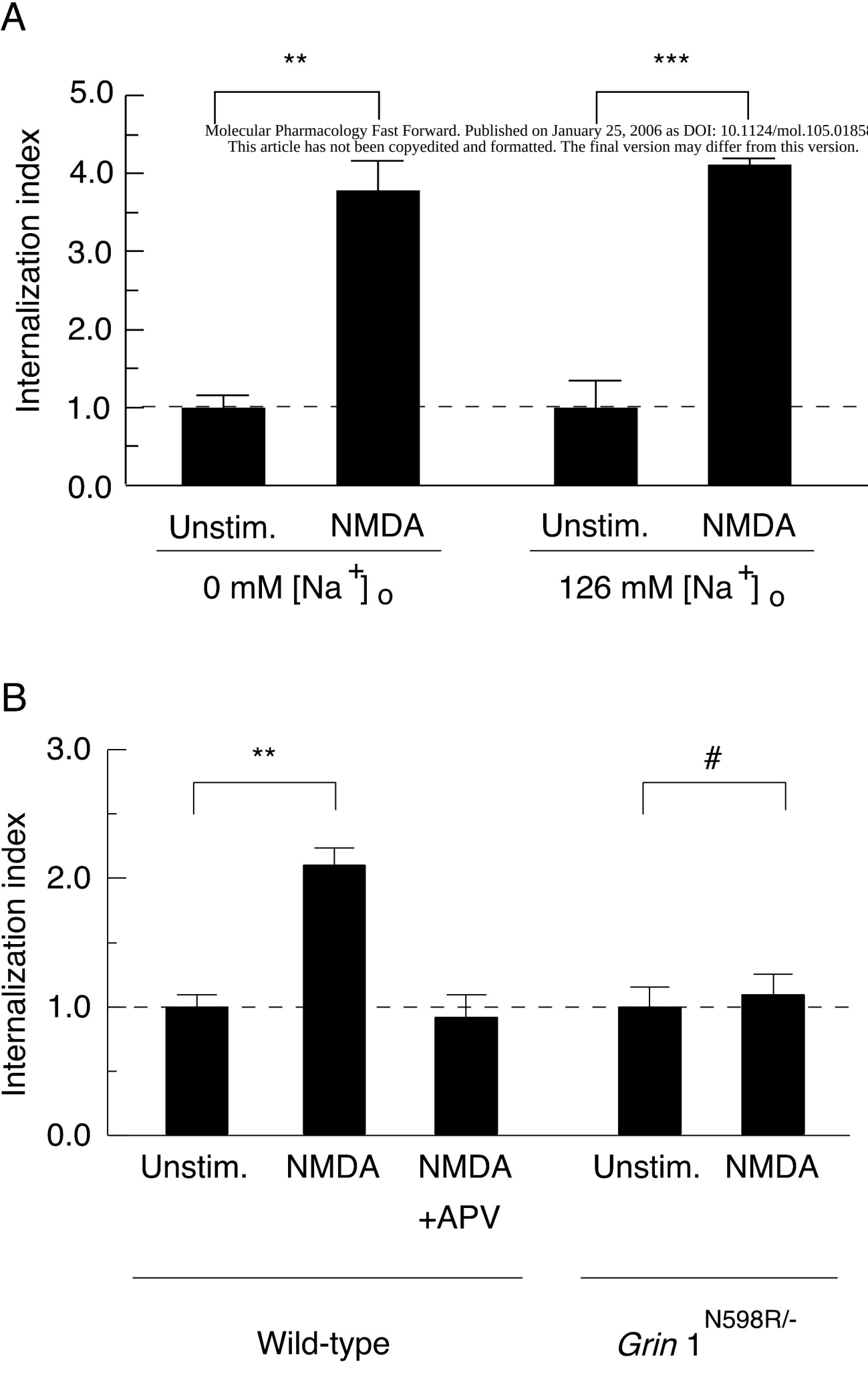

Figure 4

A

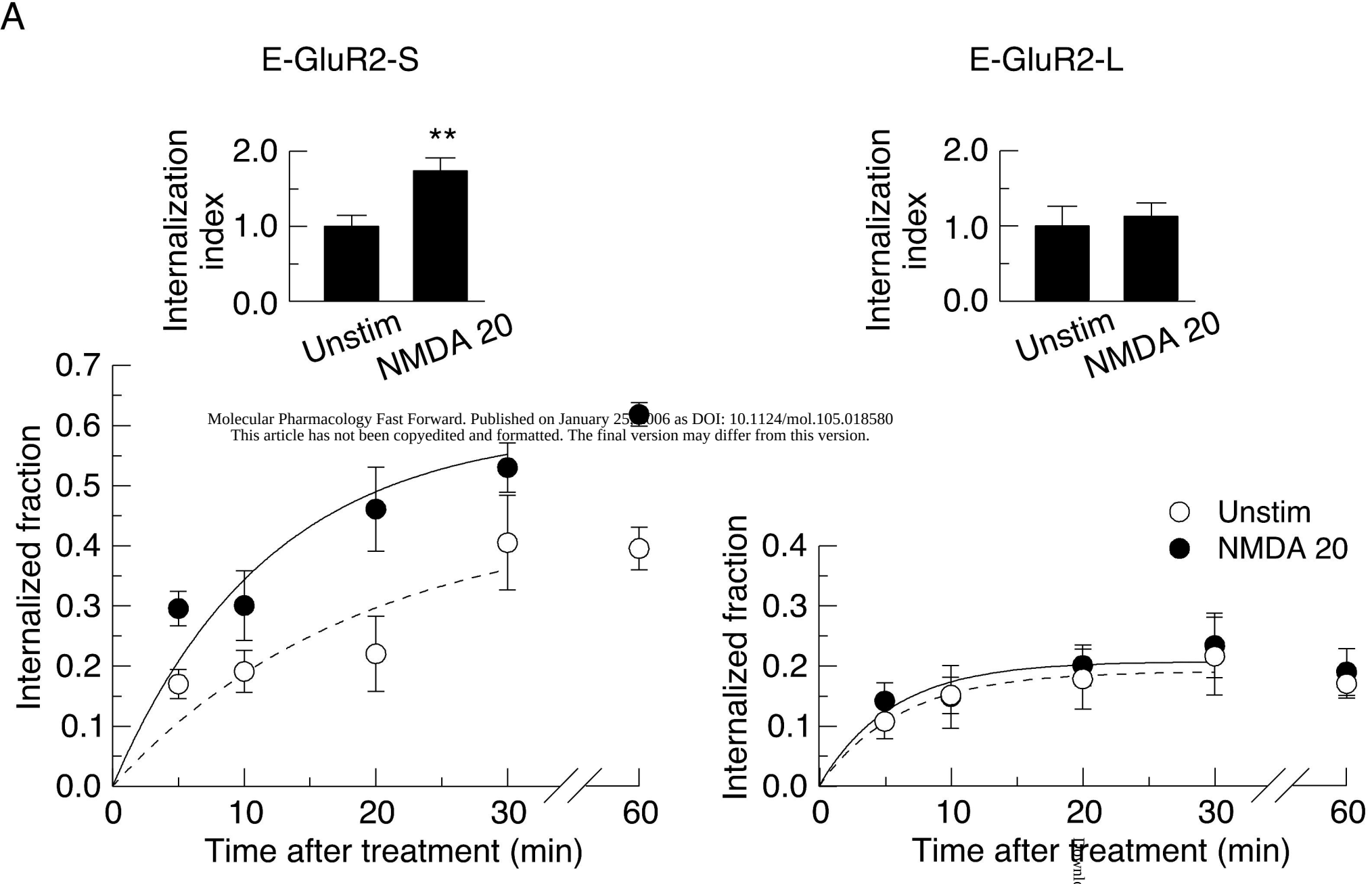

Molecular Pharmacology Fast Forward. Published on January 25, 2006 as DOI: 10.1124/mol.105.018580
This article has not been copyedited and formatted. The final version may differ from this version.

B

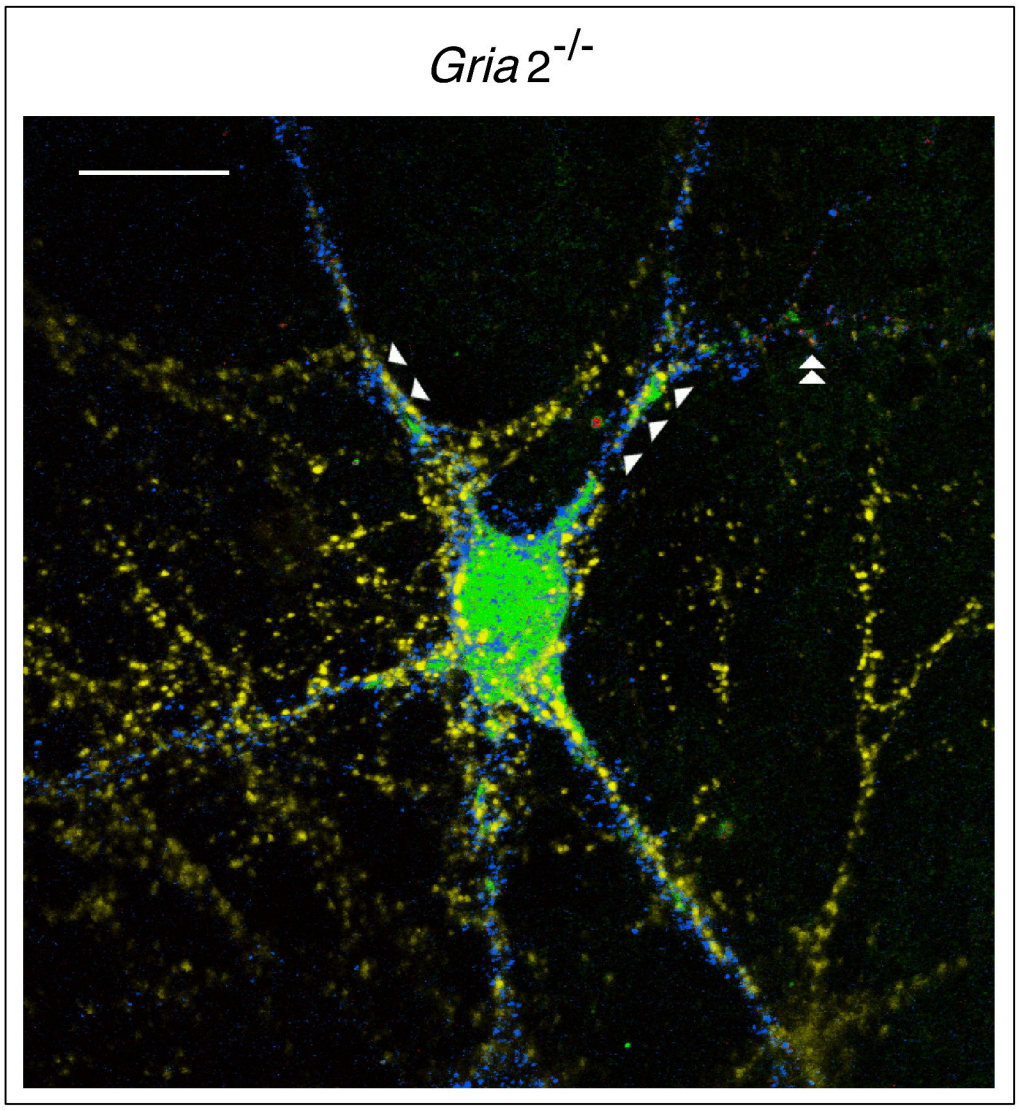

C

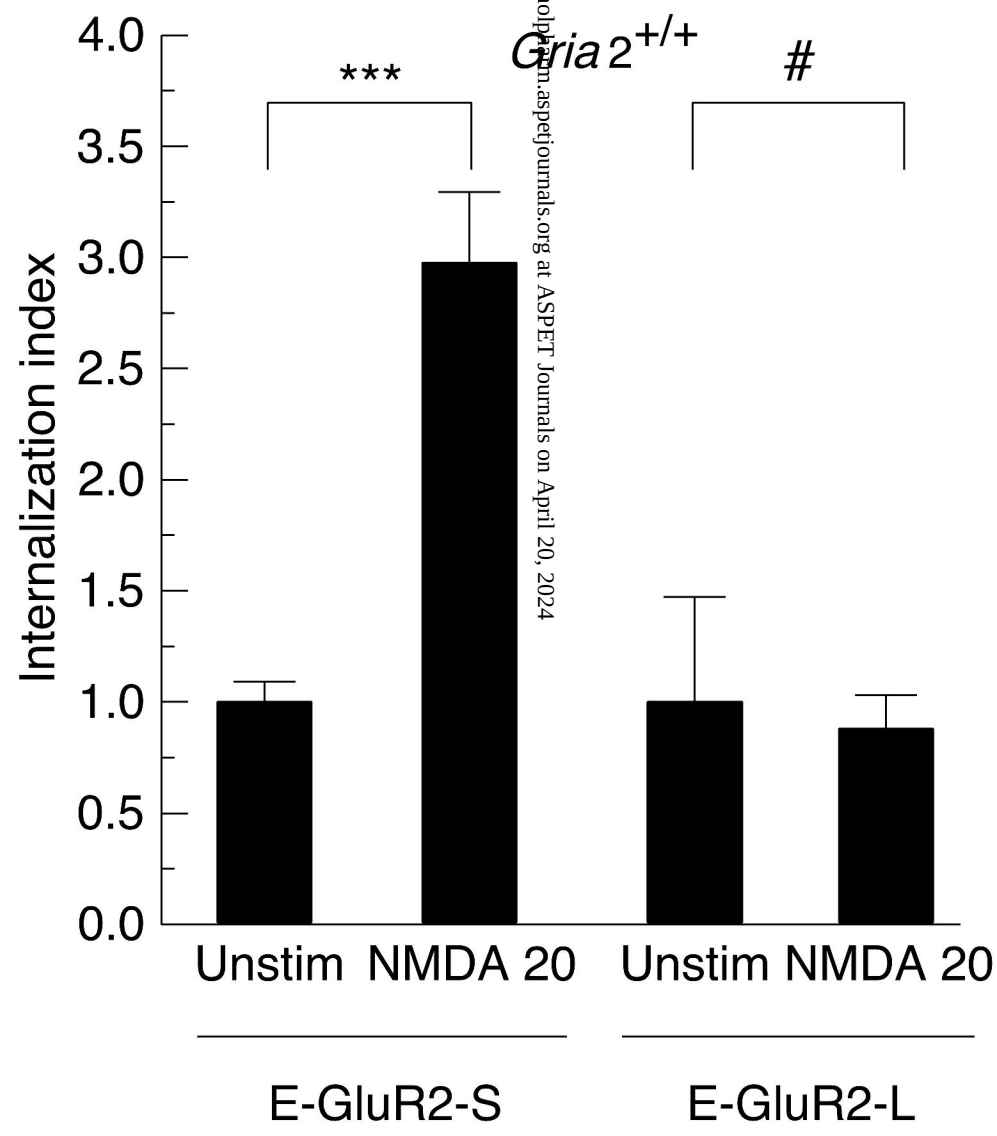

Figure 5

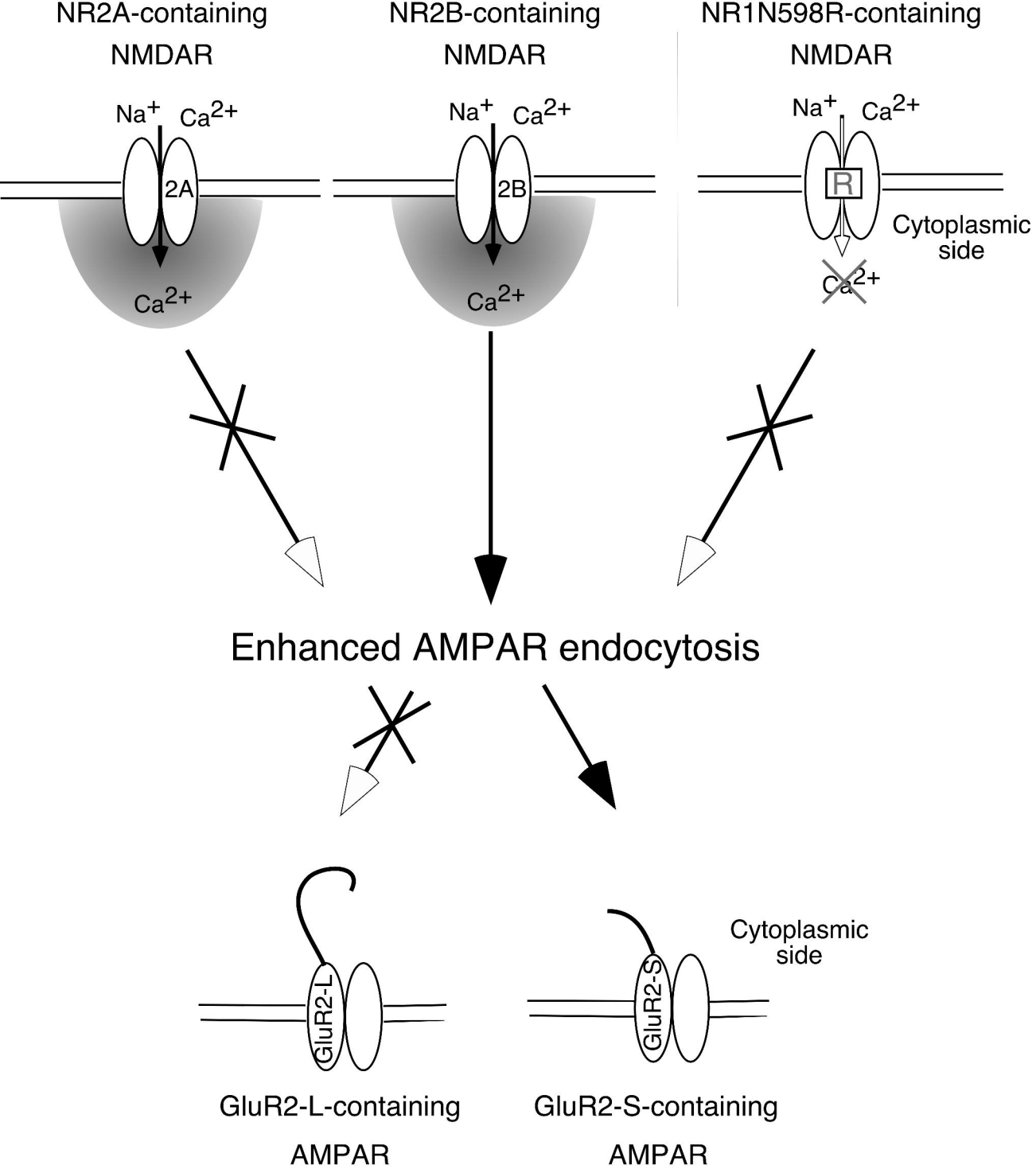
NR2A-containing
NMDAR
NR2B-containing
NMDAR
NR1N598R-containing
NMDAR
Na+ Ca2+
2A
Ca2+
Na+ Ca2+
2B
Ca2+
Na+ Ca2+
R
Cytoplasmic
side
Ca2+
Enhanced AMPAR endocytosis
GluR2-L
GluR2-L-containing
AMPAR
GluR2-S
Cytoplasmic
side
GluR2-S-containing
AMPAR

Figure 6

Supplementary Material for

Subunit dependencies of NMDA receptor-induced AMPA receptor internalization

C. M. Tigaret, A. Thalhammer, G. F. Rast, C. G. Specht, Y. P. Auberson, M. G. Stewart, and R. Schoepfer.

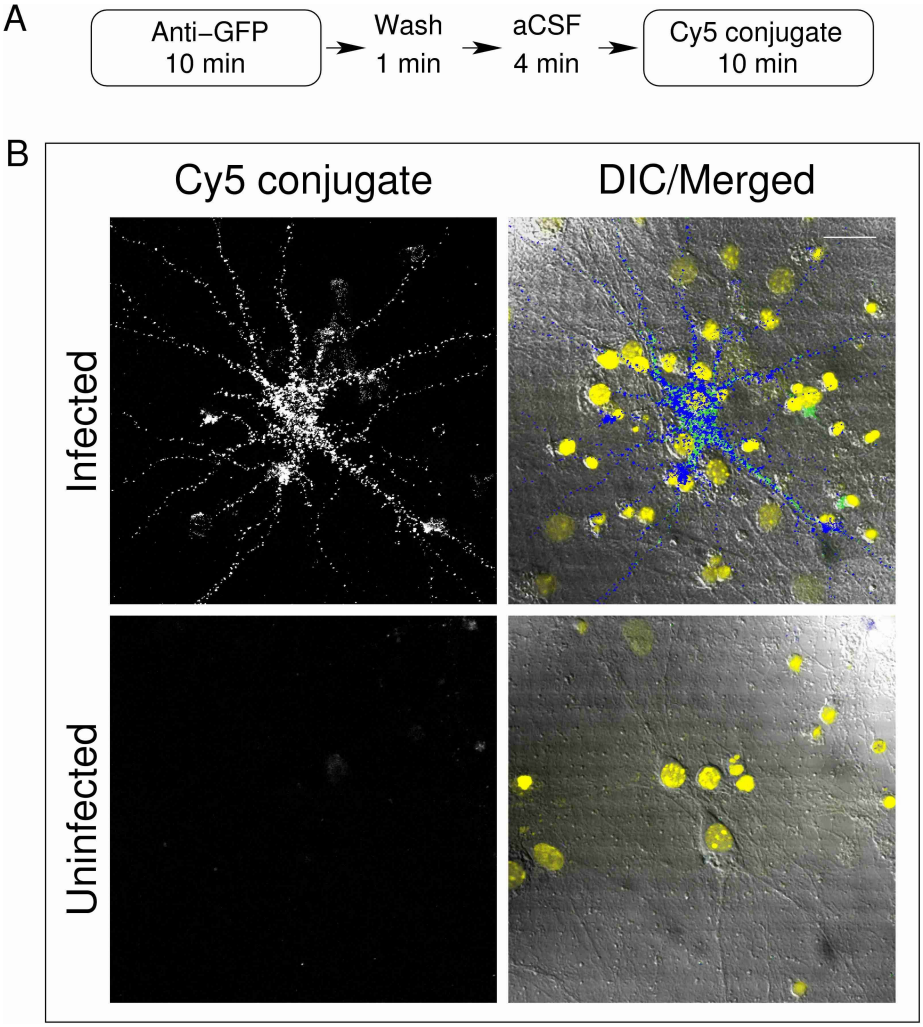

Supplementary Figure S1. Anti-GFP specificity.

Anti-GFP immunofluorescence (rabbit polyclonal anti-GFP / Cy5-conjugated anti-Rabbit IgG) for surface E-GluR2-S on hippocampal neurons from cultures infected with E-GluR2-S Sindbis virus or naïve (uninfected), performed under non-permeabilizing conditions. *A*. Scheme for the staining protocol. *B*. Fluorescence of the Cy5 channel (Cy5 conjugate) is shown next to all fluorescence channels overlayed with the DIC image of the same field (DIC/Merged).

Only the cells expressing E-GluR2-S (green) from the infected cultures yielded detectable punctated anti-GFP immunofluorescence (i.e., Cy5) signal (blue in DIC/Merged) representing surface E-GluR2-containing AMPARs. E-GluR2-S fluorescence is shown in green. Cell nuclei (yellow) were stained with 1µg/ml Hoechst 33258 (Molecular Probes, Inc) for 5 min prior to mounting. Scale bar: 20 µm.

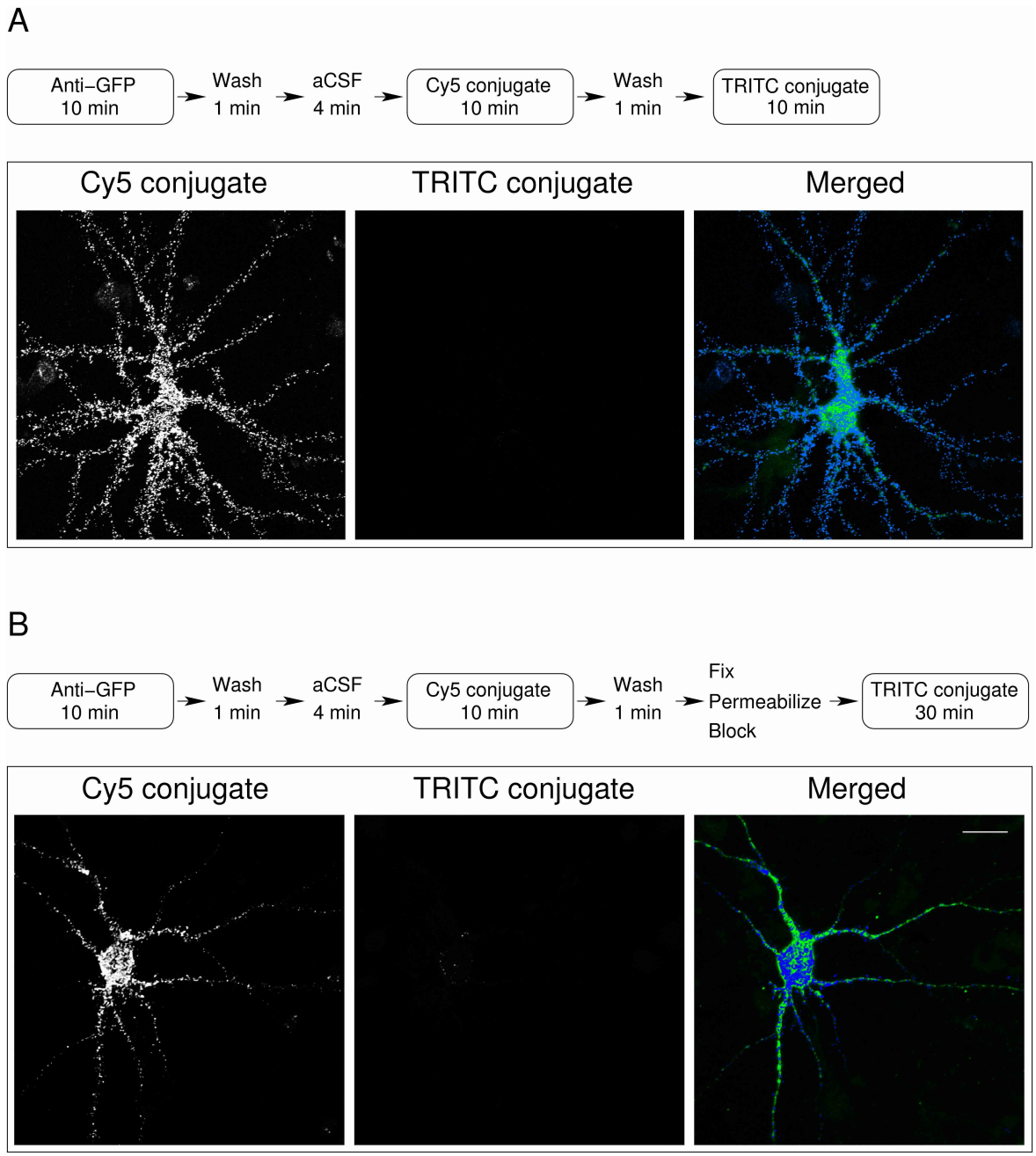

Supplementary Figure S2. Saturation of surface E-GluR2-S epitopes.

Anti-GFP immunofluorescence for E-GluR2-S-containing AMPARs with both secondary antibody conjugates applied successively on live neurons (*A*) or with the TRITC conjugate applied after fixation and permeabilization (*B*) as indicated in the staining protocol schemes at the top of the images. Z-projected confocal stacks of the individual antibody conjugate channel are shown next to the merged triple fluorescence image (green: E-GluR2-S; blue: Cy5 conjugate; red: TRITC conjugate). Scale bar: 20 µm.

The absence of a detectable TRITC signal in (*A*) indicates that the surface epitopes were saturated with the Cy5 conjugate. In (*B*) a small amount of TRITC signal was detected, which indicates that a small amount of constitutive E-GluR2-S endocytosis had occurred during the live incubations. Cell shown in A and B are representative for the quantitative data listed respectively, in rows 1 and 2 of the Supplementary Table SI.

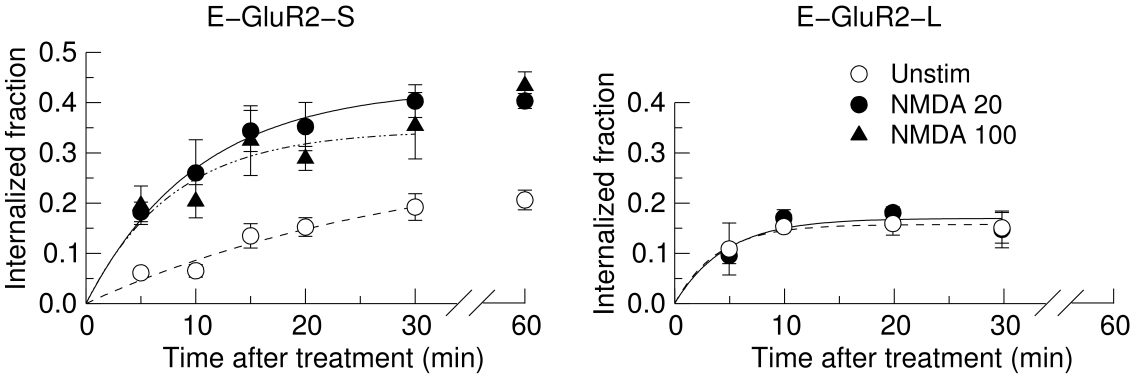

Supplementary Figure S3. Time-course of EGFP-tagged GluR2 C-terminal splice variants internalization in wild-type hippocampal neurons.

Internalized fraction of short (E-GluR2-S) and long (E-GluR2-L) C-terminal splice variants of EGFP-tagged GluR2 in wild-type neurons, plotted against the time lapsed between treatment and the live secondary antibody staining. Immunofluorescence protocol as depicted in Supplementary Table SI. Quantitative data are listed in Supplementary Table SI, as follows: cells expressing E-GluR2-S in rows 3-8 (unstimulated, Unstim.) rows 9-14 (stimulated with 20 μM NMDA + 10 μM Gly, NMDA 20) and in rows 15-20 (stimulated with 100 μM NMDA + 1 μM Gly, NMDA 100); cells expressing E-GluR2-L in rows 21-24 (Unstim.) and rows 25-28 (NMDA 20). Values represent means ± SEM. Data for time points 5-30 min were fitted to one-phase exponential association equation. Correlation coefficients of the non-linear fits were 0.97 (E-GluR2-S Unstim.), 0.95 (E-GluR2-L Unstim.), 0.99 (E-GluR2-S NMDA 20), 0.84 (E-GluR2-L NMDA 20), and 0.9 (E-GluR2-S NMDA 100). Data for time point 60 were obtained with antibody incubation times of 40 min (anti-GFP) and 30 min for the Cy5 conjugate.

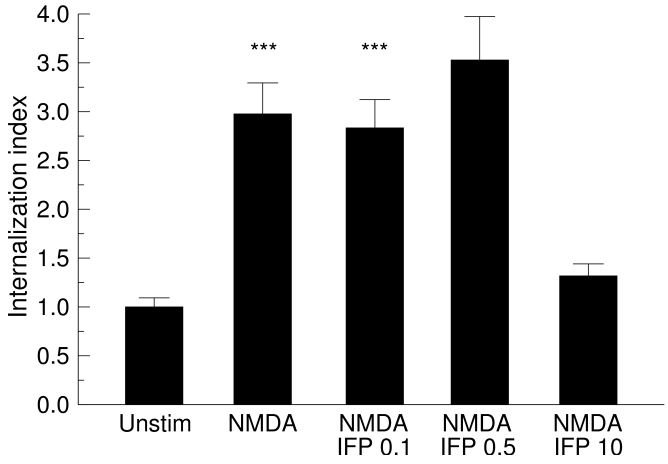

Supplementary Figure S4. Ifenprodil concentrations at and below IC50 do not inhibit NMDA-induced E-GluR2-S internalization. Internalization of E-GluR2-S in wild-type neurons was determined at 5 min after stimulation with 20 μM NMDA + 10 μM Gly. Values represent means ± SEM of internalized fraction normalized to the unstimulated mean. Raw data are given in Supplementary Table SI, rows 3, 9, 60, 61, and 62, respectively.

Supplementary Table SI

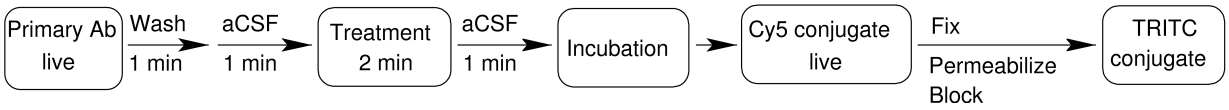

	Genotype	***GluR2 variant[a]***	***Primary Ab[b] (min)***	***Treatment (2 min)***		***Incubation (min)***	***Cy5 conjugate (min)***	***Internalized fraction***	***SEM***	***n***
				Agonist	***Antagonist***					
1	Wild-type[c]	E-GluR2-S	10			0	10	0.00	0.00	7
2	Wild-type	E-GluR2-S	10			0	10	0.01	0.01	6
3	Wild-type	E-GluR2-S	10			5	10	0.06	0.01	42
4	Wild-type	E-GluR2-S	10			10	10	0.07	0.01	12
5	Wild-type	E-GluR2-S	10			15	10	0.13	0.02	15
6	Wild-type	E-GluR2-S	10			20	10	0.15	0.02	19
7	Wild-type	E-GluR2-S	10			30	10	0.19	0.03	13
8	Wild-type	E-GluR2-S	40			60	30	0.21	0.02	52
9	Wild-type	E-GluR2-S	10	NMDA 20		5	10	0.18	0.02	46
10	Wild-type	E-GluR2-S	10	NMDA 20		10	10	0.26	0.07	4
11	Wild-type	E-GluR2-S	10	NMDA 20		15	10	0.34	0.04	10
12	Wild-type	E-GluR2-S	10	NMDA 20		20	10	0.35	0.05	15
13	Wild-type	E-GluR2-S	10	NMDA 20		30	10	0.44	0.03	5
14	Wild-type	E-GluR2-S	40	NMDA 20		60	30	0.40	0.01	5
15	Wild-type	E-GluR2-S	10	NMDA 100		5	10	0.20	0.04	9
16	Wild-type	E-GluR2-S	10	NMDA 100		10	10	0.20	0.03	6
17	Wild-type	E-GluR2-S	10	NMDA 100		15	10	0.32	0.07	6
18	Wild-type	E-GluR2-S	10	NMDA 100		20	10	0.29	0.02	7
19	Wild-type	E-GluR2-S	10	NMDA 100		30	10	0.35	0.07	8
20	Wild-type	E-GluR2-S	40	NMDA 100		60	30	0.43	0.03	46
21	Wild-type	E-GluR2-L	10			5	10	0.15	0.01	13
22	Wild-type	E-GluR2-L	10			10	10	0.11	0.05	6
23	Wild-type	E-GluR2-L	10			20	10	0.16	0.02	13
24	Wild-type	E-GluR2-L	10			30	10	0.15	0.03	10
25	Wild-type	E-GluR2-L	10	NMDA 20		5	10	0.10	0.02	9
26	Wild-type	E-GluR2-L	10	NMDA 20		10	10	0.17	0.02	23
27	Wild-type	E-GluR2-L	10	NMDA 20		20	10	0.18	0.01	5
28	Wild-type	E-GluR2-L	10	NMDA 20		30	10	0.15	0.04	7
29	*Gria2*$^{-/-}$	E-GluR2-S	10			5	10	0.17	0.02	10
30	*Gria2*$^{-/-}$	E-GluR2-S	10			10	10	0.19	0.04	5
31	*Gria2*$^{-/-}$	E-GluR2-S	10			20	10	0.22	0.06	7
32	*Gria2*$^{-/-}$	E-GluR2-S	10			30	10	0.41	0.08	7
33	*Gria2*$^{-/-}$	E-GluR2-S	40			60	30	0.40	0.04	14
34	*Gria2*$^{-/-}$	E-GluR2-S	10	NMDA 20		5	10	0.30	0.03	8
35	*Gria2*$^{-/-}$	E-GluR2-S	10	NMDA 20		10	10	0.30	0.06	8
36	*Gria2*$^{-/-}$	E-GluR2-S	10	NMDA 20		20	10	0.46	0.07	8
37	*Gria2*$^{-/-}$	E-GluR2-S	10	NMDA 20		30	10	0.53	0.04	9

	Genotype	***GluR2 variant[a]***	***Primary Ab[b] (min)***	***Treatment (2 min)***		***Incubation (min)***	***Cy5 conjugate (min)***	***Internalized fraction***	***SEM***	***n***
				Agonist	***Antagonist***					
38	*Gria2*$^{-/-}$	E-GluR2-S	40	NMDA 100		60	30	0.62	0.02	6
39	*Gria2*$^{-/-}$	E-GluR2-L	10			5	10	0.11	0.03	6
40	*Gria2*$^{-/-}$	E-GluR2-L	10			10	10	0.15	0.03	12
41	*Gria2*$^{-/-}$	E-GluR2-L	10			20	10	0.18	0.05	7
42	*Gria2*$^{-/-}$	E-GluR2-L	10			30	10	0.22	0.06	6
43	*Gria2*$^{-/-}$	E-GluR2-L	40			60	30	0.17	0.02	28
44	*Gria2*$^{-/-}$	E-GluR2-L	10	NMDA 20		5	10	0.14	0.03	5
45	*Gria2*$^{-/-}$	E-GluR2-L	10	NMDA 20		10	10	0.15	0.05	9
46	*Gria2*$^{-/-}$	E-GluR2-L	10	NMDA 20		20	10	0.20	0.03	8
47	*Gria2*$^{-/-}$	E-GluR2-L	10	NMDA 20		30	10	0.23	0.05	10
48	*Gria2*$^{-/-}$	E-GluR2-L	40	NMDA 100		60	30	0.19	0.04	10
49	Wild-type	E-GluR2-S	10		NVP 1	5	10	0.09	0.01	6
50	Wild-type	E-GluR2-S	10		NVP 1	20	10	0.18	0.02	10
51	Wild-type	E-GluR2-S	40		NVP 1	60	30	0.22	0.03	14
52	Wild-type	E-GluR2-S	10	NMDA 20	NVP 1	5	10	0.28	0.05	8
53	Wild-type	E-GluR2-S	10	NMDA 20	NVP 1	20	10	0.42	0.03	24
54	Wild-type	E-GluR2-S	40	NMDA 20	NVP 1	60	30	0.45	0.06	5
55	Wild-type	E-GluR2-S	40	NMDA 100	NVP 1	60	30	0.38	0.07	11
56	Wild-type	E-GluR2-S	10		IFP 10	20	10	0.16	0.02	7
57	Wild-type	E-GluR2-S	40		IFP 10	60	30	0.17	0.04	10
58	Wild-type	E-GluR2-S	10	NMDA 20	IFP 0.01	5	10	0.16	0.01	17
59	Wild-type	E-GluR2-S	10	NMDA 20	IFP 0.05	5	10	0.17	0.02	11
60	Wild-type	E-GluR2-S	10	NMDA 20	IFP 0.1	5	10	0.17	0.02	13
61	Wild-type	E-GluR2-S	10	NMDA 20	IFP 0.5	5	10	0.22	0.03	22
62	Wild-type	E-GluR2-S	10	NMDA 20	IFP 10	5	10	0.08	0.01	5
63	Wild-type	E-GluR2-S	10	NMDA 20	IFP 10	20	10	0.16	0.04	8
64	Wild-type	E-GluR2-S	40	NMDA 20	IFP 10	60	30	0.12	0.02	5
65	Wild-type	E-GluR2-S	40	NMDA 100	IFP 10	60	30	0.26	0.03	6
66	Wild-type	E-GluR2-S	40		Ro 1	60	30	0.21	0.02	12
67	Wild-type	E-GluR2-S	40	NMDA 100	Ro 1	60	30	0.17	0.02	14
68	Wild-type	E-GluR2-S	10		APV 50	20	10	0.14	0.01	5
69	Wild-type	E-GluR2-S	40		APV 100	60	30	0.17	0.01	3
70	Wild-type	E-GluR2-S	10	NMDA 20	APV 50	20	10	0.17	0.01	5
71	Wild-type	E-GluR2-S	40	NMDA 100	APV 100	60	30	0.19	0.04	24
72	*Grin1*$^{N598R/-}$	E-GluR2-S	40			60	30	0.40	0.06	12
73	*Grin1*$^{N598R/-}$	E-GluR2-S	40	NMDA 100		60	30	0.43	0.06	15
74	*Grin1*$^{-/-}$	E-GluR2-S	40			60	30	0.50	0.05	21
75	Wild-type[(d)]	E-GluR2-S	10	0 mM $[Na^+]_o$		5	10	0.07	0.02	10
76	Wild-type[(d)]	E-GluR2-S	40	0 mM $[Na^+]_o$		60	30	0.16	0.03	10
77	Wild-type[(d)]	E-GluR2-S	10	0 mM $[Na^+]_o$ NMDA 20		5	10	0.28	0.07	6
78	Wild-type[(d)]	E-GluR2-S	40	0 mM $[Na^+]_o$ NMDA 100		60	30	0.34	0.06	6
79	Wild-type[(d)]	E-GluR2-S	10	126 mM $[Na^+]_o$		5	10	0.07	0.02	9

	Genotype	***GluR2 variant[(a)]***	***Primary Ab[(b)] (min)***	***Treatment (2 min)***		***Incubation (min)***	***Cy5 conjugate (min)***	***Internalized fraction***	***SEM***	***n***
				Agonist	***Antagonist***					
80	Wild-type[(d)]	E-GluR2-S	40	126 mM $[Na^+]_o$		60	30	0.17	0.04	7
81	Wild-type[(d)]	E-GluR2-S	10	126 mM $[Na^+]_o$ NMDA 20		5	10	0.30	0.04	7
82	Wild-type[(d)]	E-GluR2-S	40	126 mM $[Na^+]_o$ NMDA 100		60	30	0.29	0.03	11
83	Wild-type	Endo	10			5	10	0.08	0.01	19
84	Wild-type	Endo	10	NMDA 20		5	10	0.21	0.03	17
85	Wild-type	Endo	10		APV 50	5	10	0.09	0.03	7
86	Wild-type	Endo	10	NMDA 20	APV 50	5	10	0.08	0.01	8
87	Wild-type	Endo	10		IFP 10	5	10	0.09	0.01	19
88	Wild-type	Endo	10	NMDA 20	IFP 1	5	10	0.11	0.01	6
89	Wild-type	Endo	10	NMDA 20	IFP 10	5	10	0.10	0.02	19
90	Wild-type	Endo	10		NVP 1	5	10	0.09	0.01	19
91	Wild-type	Endo	10	NMDA 20	NVP 1	5	10	0.26	0.04	20

Supplementary Table SI. Absolute values for the internalized fraction of GluR2-AMPARs in all the experimental conditions described in the main text.

Top: scheme of the immunofluorescence staining protocol used for the detection of GluR2 internalization, see also Materials and Methods in the main text. The durations of the live antibody incubations as well as of the incubation after treatment are shown in the corresponding table columns. Surface immunocomplexes were always detected with a Cy5-conjugated antibody; internalized immunocomplexes were detected with a secondary antibody conjugated to TRITC (E-GluR2-S and E-GluR2-L) or to Cy3 (endogenous GluR2). Internalized fractions are expressed as ratio between the internalized and the surface+internalized fluorescence signals. The values in the last column are the numbers of cells analyzed for the given condition. Unless specified, all concentrations are expressed in μM, and times are expressed in minutes. NMDA 20: 20 μM NMDA + 10 μM Gly; NMDA 100: 100 μM NMDA + 1 μM Gly.

[(a)]GluR2 internalization was determined for the recombinant EGFP-tagged GluR2 C-terminal splice variants (E-GluR2-S and E-GluR2-L) or for the native, endogenous GluR2 (Endo).

[(b)]Primary antibody: anti-GFP for E-GluR2-S and E-GluR2-L, or anti-GluR2 MAB397 for the endogneous GluR2.

[(c)]Both secondary antibody conjugates were successively applied live for 10 min each (i.e., no fixation between the first and second conjugated antibodies, see Supplementary Figure S2A for examples). In all other conditions, the second conjugated antibody was applied after fixation and permeabilization, to reveal the internalized immunocomplexes.

[(d)]Experiments were performed using HEPES-based Ringer solution (see Materials and Methods in the main text).